

Phenomenology of 3-3-1 models with radiative inverse seesaw mechanism

V. H. Binh,^{1,*} Cesar Bonilla,² A. E. Cárcamo Hernández,^{3,4,5,†} D. T. Huong,^{1,‡}
Vishnudath K. N.,^{3,§} H. N. Long,^{6,7,¶} P. N. Thu,^{8,9,**} and Iván Schmidt^{3,4,5}

¹*Institute of Physics, Vietnam Academy of Science and Technology, 10 Dao Tan, Ba Dinh, Hanoi, Vietnam*

²*Departamento de Física, Universidad Católica del Norte,
Avenida Angamos 0610, Casilla 1280, Antofagasta, Chile^{††}*

³*Universidad Técnica Federico Santa María, Casilla 110-V, Valparaíso, Chile*

⁴*Centro Científico-Tecnológico de Valparaíso, Casilla 110-V, Valparaíso, Chile*

⁵*Millennium Institute for Subatomic Physics at High-Energy Frontier (SAPHIR), Fernández Concha 700, Santiago, Chile*

⁶*Subatomic Physics Research Group, Science and Technology Advanced Institute,
Van Lang University, Ho Chi Minh City, Vietnam*

⁷*Faculty of Applied Technology, School of Technology,
Van Lang University, Ho Chi Minh City, Vietnam*

⁸*Graduate University of Science and Technology, Vietnam Academy of Science and Technology,
18 Hoang Quoc Viet, Cau Giay, Hanoi, 10000, Vietnam*

⁹*Faculty of Natural Sciences - Technology, Tay Bac University,
Quyet Tam Ward, Son La City, Son La 360000, Vietnam*

We propose two models based on the $SU(3)_C \times SU(3)_L \times U(1)_X$ gauge symmetry, each incorporating distinct inverse seesaw mechanisms for generating neutrino masses at the radiative level. Therefore, neutrino masses are suppressed by the radiative nature of the mass generation mechanism, which occurs after the spontaneous breaking of the global lepton number symmetry. Both scenarios discussed here are characterized by the presence of vector-like charged leptons, which are involved in generating the masses of the Standard Model charged leptons. These additional vector-like fermions contribute to the anomalous magnetic moments of the electron and the muon. We perform a detailed analysis of the scalar sectors, show that these models can successfully accommodate the observed baryon asymmetry through resonant leptogenesis, and compute charged lepton flavor-violating decays, such as $\mu \rightarrow e\gamma$. We discuss the constraints of the model arising from these processes and those associated the non-unitarity of the lepton mixing matrix.

I. INTRODUCTION

The Standard Model (SM) of particle physics is an extremely successful theory whose predictions are highly consistent with the data from various experiments. However, it still has a few limitations that motivate one to consider theories beyond the Standard Model (BSM). One of them is the absence of a neutrino mass generation mechanism. The existence of non-zero neutrino masses has been confirmed by several neutrino oscillation experiments [1–3]. Furthermore, the SM neither explains the observed dark matter relic abundance nor the matter-antimatter asymmetry of the Universe [4]. In addition, the SM also fails to explain the features such as the existence of three generations of fermions, electric charge quantization, and the observed hierarchy among the masses of the charged fermions. All of these point towards the need for a new theory, of which the SM can be considered as a low-energy effective theory.

Current theoretical frameworks are constructed with the aim of addressing some of the issues as mentioned above. One such framework involves extensions based on the $SU(3)_C \times SU(3)_L \times U(1)_X$ gauge group (known as 3-3-1 models).

¹ Our friend and collaborator Iván Schmidt passed away during the completion of this work. He will be sorely missed.

*Electronic address: vhbinh@iop.vast.vn

†Electronic address: antonio.carcamo@usm.cl

‡Electronic address: dthuong@iop.vast.vn

§Electronic address: vishnudath.neelakand@usm.cl

¶Electronic address: hoangngoclong@vlu.edu.vn

**Electronic address: thupn@utb.edu.vn

††Electronic address: cesar.bonilla@ucn.cl

These models are of great interest because they explain the number of SM fermion families as well as the quantization of the electric charge [5, 6]. These scenarios are characterized by providing additional sources of CP-violation [7, 8] as well as a natural Peccei-Quinn symmetry, which solves the Strong-CP problem [9–12]. In addition, the 3-3-1 models also predict that the weak mixing angle θ_W has the following upper bound, $\sin \theta_W^2 < \frac{1}{4}$. Moreover, incorporating heavy sterile neutrinos into the fermion spectrum of 3-3-1 models may facilitate the emergence of potential candidates for cold dark matter, such as weakly interacting massive particles (WIMPs) [13–16]. A concise review of WIMPs in 3-3-1 electroweak gauge models is given in Ref. [17].

In 3-3-1 models, with the addition of extra Majorana neutrino gauge singlets, one can also incorporate a low-scale testable version of the traditional type-I seesaw mechanism for neutrino mass generation [18–21]. The advantage of the low-scale seesaw models such as the inverse or linear seesaw is that one can lower the scale of heavy particles without having to consider extremely small Yukawa couplings. This, in turn, makes these models testable in collider experiments. Typically, this is achieved by decoupling the scale of the seesaw from the scale of the lepton number violation. For instance, in the case of the inverse seesaw mechanism, the scale of lepton number violation usually corresponds to a small soft-breaking Majorana mass term for the exotic neutral fermions, which is $\sim \mathcal{O}(\text{keV})$, whereas the mass scale of the seesaw mediators is around $\sim \mathcal{O}(\text{TeV})$. Such models can lead to large unitarity violations of the leptonic mixing matrix that can be probed in neutrino oscillation experiments, as well sizeable rates for charged lepton flavor violating decays, such as $\mu \rightarrow e\gamma$. Moreover, the small mass splitting between the heavy pseudo-Dirac neutral leptons in these low-scale seesaw realizations facilitates a viable scenario for resonant leptogenesis [22–31]. Low scale seesaw in the context of 3-3-1 models have been studied earlier in [32–40].

In this work, we propose two models based on the $SU(3)_C \times SU(3)_L \times U(1)_X$ gauge symmetry, featuring distinct radiative inverse seesaw realization for the generation of the tiny neutrino masses. In both models, the Majorana mass submatrix associated with the breaking of the lepton number by two units is radiatively generated, thereby explaining the small neutrino masses. In the first model, the inverse seesaw mechanism is implemented at a one-loop level, whereas in the second one, the neutrino mass generation mechanism is realized at a two-loop level. It's worth noting that the one-loop inverse seesaw model proposed here is, as far as we know, the most economical realization within the context of 3-3-1 models found in the literature. Furthermore, the model exhibits a preserved Z_2 symmetry arising from the spontaneous breaking of the global lepton number symmetry, which guarantees the radiative nature of the inverse seesaw. In both models, the one- and two-loop realizations, the SM-charged fermion masses arise from a tree-level seesaw mechanism mediated by the exchange of heavy charged vector-like leptons. These vector-like fermions also contribute to the anomalous magnetic moments of the muon and the electron, thus providing a natural link between the charged lepton mass generation mechanism and the $g - 2$ anomalies. The layout of the remainder of the paper is as follows: Sec. II discusses the symmetry and particle spectra of the two models, while their scalar sectors are studied in Sec. III.

The phenomenological consequences of these models for leptogenesis, charged lepton flavor violation, and the muon and electron anomalous magnetic moments are discussed in Sections IV and V. Finally, we summarise and discuss the results in Sec. VI.

II. THE MODELS

In what follows we present two different setups based on the $SU(3)_C \times SU(3)_L \times U(1)_X$ gauge symmetry where the neutrino masses are generated via an inverse seesaw mechanism at the loop level. In such a scenario, left-handed fermions are in triplet representations of $SU(3)_L$ hence, anomaly gauge cancellation is guaranteed. For this reason, these models offer a good explanation for the number of SM fermion families in nature. Another interesting result related to anomaly cancellation in these frameworks is the quantization of electric charge [6].

On the other hand, lacking the mechanism chosen by nature to account for small neutrino masses, the inverse seesaw mechanism [18–21, 41] turns out to be appealing given the rich phenomenology [28, 30, 31, 42–46]. The neutrino mass matrix, in this case, has the following structure

$$M_\nu = \begin{pmatrix} 0_{3 \times 3} & m & 0_{3 \times 3} \\ m^T & 0_{3 \times 3} & M \\ 0_{3 \times 3} & M^T & \mu \end{pmatrix}. \quad (1)$$

in the basis (ν_L, ν_R^C, N_R^C) . There are nine neutral fermions, three active neutrinos ν_{iL} , and six ν_{iR} and N_{iR} (with $i = 1, 2, 3$) sterile neutrinos. Hence, M_ν turns out to be a 9×9 matrix. Assuming that the submatrices in Eq. (1)

satisfy the hierarchy $\mu \ll m \ll M$ the light neutrino mass matrix is

$$m_\nu = m(M^T)^{-1}\mu M^{-1}m^T.$$

From the last equation, one can see that the smallness of the neutrino masses is regulated by the linear dependence of the parameter μ . That is, if $\mu \rightarrow 0$ then $m_\nu = 0$, implying lepton number conservation. One can argue that μ has a radiative origin and that the submatrices m and M arise at the tree level. This could lead to an explanation of the hierarchy $\mu \ll m \ll M$, and hence the small neutrino masses.

A. Model-1: 3-3-1 model with inverse seesaw at one-loop

We consider a theory with the gauge symmetry $SU(3)_C \times SU(3)_L \times U(1)_X$ supplemented by two global symmetries, a generalized global lepton number $U(1)_{L_g}$ and a discrete Z_2 symmetry. We will consider the situation in which both, gauge and global, symmetry groups are broken after spontaneous symmetry breaking. The scalar sector of the model consists of three $SU(3)_L$ scalar triplets χ , η and ρ , as well as three electrically neutral gauge singlet scalars φ , σ , ξ . The $SU(3)_L$ scalar triplet χ triggers the spontaneous breaking of the $SU(3)_L \times U(1)_X$ symmetry down to the SM electroweak gauge group, which is further broken spontaneously by the $SU(3)_L$ scalar triplets η and ρ .

The fermion sector of the model under consideration includes: the fermionic particles of the conventional 3-3-1 model with right-handed neutrinos, three charged vector-like leptons E_i ($i = 1, 2, 3$) and two additional neutral leptons Ψ_{nR} ($n = 1, 2$), transforming as singlets under the $SU(3)_L$. In this scenario, it is expected a mix between the charged vector-like leptons E_i and the SM-charged leptons, thereby triggering an extended seesaw mechanism that generates the SM-charged lepton masses. Additionally, these vector-like leptons E_i induce contributions to the muon and electron anomalous magnetic moments at the one-loop level. We summarize in Tables I, II, and III the particle content along with the charge assignments under the symmetries of the model.

	$SU(3)_C$	$SU(3)_L$	$U(1)_X$	$U(1)_{L_g}$	Z_2
χ	1	3	$-\frac{1}{3}$	$\frac{4}{3}$	-1
η	1	3	$-\frac{1}{3}$	$-\frac{2}{3}$	1
ρ	1	3	$\frac{2}{3}$	$-\frac{2}{3}$	1
φ	1	1	0	$-\frac{1}{2}$	1
σ	1	1	0	1	1
ξ	1	1	0	0	-1

Table I: Charge assignments of the scalar fields under $SU(3)_C \times SU(3)_L \times U(1)_X \times U(1)_{L_g} \times Z_2$ for Model-1.

	$SU(3)_C$	$SU(3)_L$	$U(1)_X$	$U(1)_{L_g}$	Z_2
Q_{nL}	3	$\bar{\mathbf{3}}$	0	$\frac{2}{3}$	1
Q_{3L}	3	3	$\frac{1}{3}$	$-\frac{2}{3}$	1
u_{iR}	3	1	$\frac{2}{3}$	0	1
d_{iR}	3	1	$-\frac{1}{3}$	0	1
T_R	3	1	$\frac{2}{3}$	-2	-1
B_{nR}	3	1	$-\frac{1}{3}$	2	-1

Table II: Charge assignments of the quarks under $SU(3)_C \times SU(3)_L \times U(1)_X \times U(1)_{L_g} \times Z_2$ for Model-1.

Notice that neutral leptons Ψ_{nR} ($n = 1, 2$) induce a one-loop level Majorana mass term for the gauge singlet neutral fermions N_{iR} (the μ term in Eq. 1), thus giving rise to an inverse seesaw mechanism at one-loop level. The breaking of generalized global lepton number, $U(1)_{L_g}$ symmetry, into a residual \tilde{Z}_2 -symmetry is also relevant for this mechanism to work. This is evident from the transformations of the fields under the preserved \tilde{Z}_2 symmetry, defined as $(-1)^{6L}$, with L being the global lepton number. This implies that the fields N_{iR} , φ , and Ψ_{nR} carrying a non-trivial charge under $U(1)_{L_g}$ transform as under the residual symmetry as \tilde{Z}_2 -odd, whereas the remaining fields

	$SU(3)_C$	$SU(3)_L$	$U(1)_X$	$U(1)_{L_g}$	Z_2
L_{iL}	1	3	$-\frac{1}{3}$	$\frac{1}{3}$	-1
l_{iR}	1	1	-1	1	1
E_{iL}	1	1	-1	1	-1
E_{iR}	1	1	-1	1	-1
N_{iR}	1	1	0	-1	1
Ψ_{nR}	1	1	0	$\frac{1}{2}$	1

Table III: Charge assignments of the leptons under $SU(3)_C \times SU(3)_L \times U(1)_X \times U(1)_{L_g} \times Z_2$ for Model-1.

are \tilde{Z}_2 -even. See Appendix A for more details about the operators required to successfully generate μ at the loop level.

In this model, the lepton number is defined as [47]:

$$L = \frac{4}{\sqrt{3}}T_8 + L_g, \quad (2)$$

where L_g corresponds to the generalized lepton number [33]. As mentioned, the remnant preserved \tilde{Z}_2 symmetry allows for the implementation of a one-loop level inverse seesaw mechanism that produces the tiny active neutrino masses. The electric charge in the considered model is given by the expression:

$$Q = T_3 - \frac{1}{\sqrt{3}}T_8 + X,$$

where T_3 and T_8 are the $SU(3)_L$ generators and X is the $U(1)_X$ charge.

The fermion representations of the $SU(3)_L$ group are organized as follows:

$$Q_{1L} = \begin{pmatrix} u_1 \\ d_1 \\ J_1 \end{pmatrix}_L \sim \left(\mathbf{3}, \mathbf{3}, \frac{1}{3} \right), \quad Q_{nL} = \begin{pmatrix} d_n \\ -u_n \\ J_n \end{pmatrix}_L \sim (\mathbf{3}, \bar{\mathbf{3}}, 0), \quad L_{iL} = \begin{pmatrix} \nu_i \\ l_i \\ \nu_i^c \end{pmatrix}_L \sim \left(\mathbf{1}, \mathbf{3}, -\frac{1}{3} \right).$$

The $SU(3)_L$ scalar triplets of this model are represented as:

$$\rho = \begin{pmatrix} \rho_1^+ \\ \frac{1}{\sqrt{2}}(v_\rho + R_\rho + iI_\rho) \\ \rho_3^+ \end{pmatrix}, \quad \eta = \begin{pmatrix} \frac{1}{\sqrt{2}}(v_\eta + R_\eta^1 + iI_\eta^1) \\ \eta_2^- \\ R_\eta^3 + iI_\eta^3 \end{pmatrix}, \quad \chi = \begin{pmatrix} R_\chi^1 + iI_\chi^1 \\ \chi_2^- \\ \frac{1}{\sqrt{2}}(v_\chi + R_\chi^3 + iI_\chi^3) \end{pmatrix} \quad (3)$$

and the singlet scalars introduced to this model are:

$$\varphi = \frac{1}{\sqrt{2}}(R_\varphi + iI_\varphi), \quad \xi = \frac{1}{\sqrt{2}}(v_\xi + R_\xi), \quad \sigma = \frac{1}{\sqrt{2}}(v_\sigma + R_\sigma + iI_\sigma). \quad (4)$$

The singlet scalar ξ is a real field that acquires a VEV. Further, both φ and σ are complex fields among which only σ gets a non-zero value of VEV.

With the above-specified particle content and symmetries, the following Yukawa terms emerge for the quark and lepton sectors:

$$\begin{aligned} -\mathcal{L}_Y^{(q)} = & \sum_{n=1}^2 \sum_{i=1}^3 (y_u)_{ni} \bar{Q}_{nL} \rho^* u_{iR} + \sum_{i=1}^3 (y_u)_{3i} \bar{Q}_{3L} \eta u_{iR} \\ & + \sum_{n=1}^2 \sum_{i=1}^3 (y_d)_{ni} \bar{Q}_{nL} \eta^* d_{iR} + \sum_{i=1}^3 (y_d)_{3i} \bar{Q}_{3L} \rho d_{iR} \\ & + \sum_{n=1}^2 \sum_{k=1}^2 (y_B)_{nk} \bar{Q}_{nL} \chi^* B_{kR} + y_T \bar{Q}_{3L} \chi T_R + H.c \end{aligned} \quad (5)$$

$$\begin{aligned}
-\mathcal{L}_Y^{(l)} = & \sum_{i=1}^3 \sum_{j=1}^3 y_{ij}^{(E)} \bar{L}_{iL} \rho E_{jR} + \sum_{i=1}^3 \sum_{j=1}^3 y_{ij}^{(l)} \bar{E}_{iL} \xi l_{jR} + \sum_{i=1}^3 \sum_{j=1}^3 (m_E)_{ij} \bar{E}_{iL} E_{jR} \\
& + \frac{1}{2} \sum_{i=1}^3 \left(x_\rho^{(L)} \right)_{ij} \varepsilon_{abc} \bar{L}_{iL}^a (L_{jL}^C)^b (\rho^*)^c + \sum_{i=1}^3 \sum_{j=1}^3 (y_N)_{ij} \bar{L}_{iL} \chi N_{jR} \\
& + \sum_{i=1}^3 \sum_{n=1}^2 (y_N)_{in} \bar{N}_{iR} \Psi_{nR}^C \varphi + \sum_{n=1}^2 \sum_{m=1}^2 (y_\Psi)_{nm} \bar{\Psi}_{nR} \sigma \Psi_{mR}^C + H.c
\end{aligned} \tag{6}$$

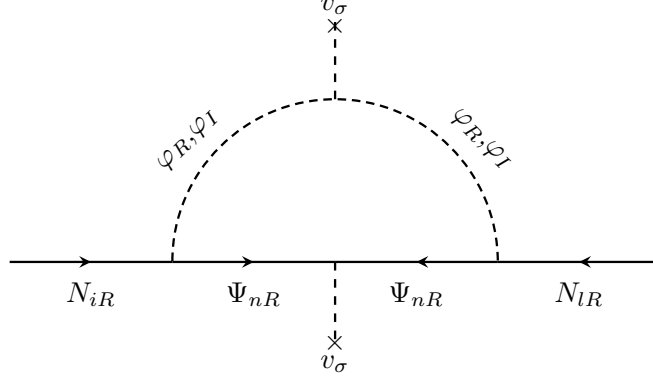


Figure 1: One-loop Feynman diagram contributing to the Majorana neutrino mass submatrix μ in model 1.

The neutrino Yukawa interactions yield the following neutrino mass terms:

$$-\mathcal{L}_{mass}^{(\nu)} = \frac{1}{2} \left(\bar{\nu}_L^C \quad \bar{\nu}_R \quad \bar{N}_R \right) M_\nu \begin{pmatrix} \nu_L \\ \nu_R^C \\ N_R^C \end{pmatrix} + \frac{1}{2} \sum_{n=1}^2 \sum_{m=1}^2 (m_\Psi)_{nm} \bar{\Psi}_{nR} \Psi_{mR}^C + H.c, \tag{7}$$

where $m_\Psi = \sqrt{2} y_\Psi v_\sigma$ and the neutrino mass matrix M_ν has the form:

$$M_\nu = \begin{pmatrix} 0_{3 \times 3} & m & 0_{3 \times 3} \\ m^T & 0_{3 \times 3} & M \\ 0_{3 \times 3} & M^T & \mu \end{pmatrix}, \tag{8}$$

with the neutrino submatrices m , M and μ given by:

$$\begin{aligned}
m &= \frac{v_\rho}{\sqrt{2}} \left[\left(x_\rho^{(L)} \right)^\dagger - \left(x_\rho^{(L)} \right)^* \right], & M &= \sqrt{2} y_N v_\chi, \\
\mu_{sp} &= \sum_{k=1}^2 \frac{(y_N)_{sk} (y_N^T)_{kp} m_{\Psi_k}}{16\pi^2} \left[\frac{m_{R_\varphi}^2}{m_{R_\varphi}^2 - m_{\Psi_k}^2} \ln \left(\frac{m_{R_\varphi}^2}{m_{\Psi_k}^2} \right) - \frac{m_{I_\varphi}^2}{m_{I_\varphi}^2 - m_{\Psi_k}^2} \ln \left(\frac{m_{I_\varphi}^2}{m_{\Psi_k}^2} \right) \right],
\end{aligned} \tag{9}$$

where the masses of the real and imaginary parts of φ are given by the Eq.(39) and Eq.(31). The one-loop diagram that generates the μ term given above is shown in Fig. 1.

B. Model-2: 3-3-1 model with inverse seesaw at two-loops

Now we discuss our second model, which is also based on the gauge $SU(3)_C \times SU(3)_L \times U(1)_X$ supplemented by the spontaneously broken $U(1)_{L_g}$ global lepton number symmetry. As in the case of Model-1, the spontaneous breaking of the $U(1)_{L_g}$ global lepton number symmetry gives rise to a remnant \tilde{Z}_2 symmetry. This \tilde{Z}_2 symmetry is assumed

to be preserved and this prevents the inverse seesaw mechanism at the tree level. The charges of fields under the \tilde{Z}_2 symmetry are given as $(-1)^{3L}$, where L corresponds to the $U(1)_{L_g}$ charge of the particle under consideration. In the proposed theory, the inverse seesaw mechanism generates the tiny masses of the light-active neutrinos, implemented at a two-loop level.

The scalar sector of the model under consideration is composed of three $SU(3)_L$ scalar triplets ρ , η and χ as given in Eq.(3), four electrically charged scalar singlets ζ^\pm , ξ^\pm and three singlet neutral complex scalars given below:

$$\sigma = \frac{1}{\sqrt{2}}(v_\sigma + R_\sigma + iI_\sigma), \quad \phi = \frac{1}{\sqrt{2}}(v_\phi + R_\phi + iI_\phi), \quad \varphi = \frac{1}{\sqrt{2}}(R_\varphi + iI_\varphi). \quad (10)$$

Among the three singlet scalars, both ϕ and σ acquire non-zero VEVs but φ does not.

The fermion content of the model remains the same as in the previous model where the inverse seesaw mechanism was implemented at one loop level. As before, the spontaneously broken $U(1)_{L_g}$ lepton number symmetry serves to forbid the charged lepton, Yukawa operator $\bar{L}_{iL}\rho l_{jR}$ so that the SM charged lepton masses are only generated from an extended seesaw-like mechanism mediated by heavy charged vector-like leptons E_i ($i = 1, 2, 3$). Moreover, the $U(1)_{L_g}$ symmetry allows for the implementation of the inverse seesaw mechanism at the two-loop level.

The scalar, quark, and leptonic spectra of the model, along with their assignments under the symmetries, are shown in Tables IV, V, and VI, respectively.

	$SU(3)_C$	$SU(3)_L$	$U(1)_X$	$U(1)_{L_g}$
χ	1	3	$-\frac{1}{3}$	$\frac{4}{3}$
η	1	3	$-\frac{1}{3}$	$-\frac{2}{3}$
ρ	1	3	$\frac{2}{3}$	$-\frac{2}{3}$
σ	1	1	0	4
ϕ	1	1	0	10
φ	1	1	0	1
ζ^\pm	1	1	± 1	∓ 3
ξ^\pm	1	1	± 1	± 5

Table IV: Scalar assignments under $SU(3)_C \times SU(3)_L \times U(1)_X \times U(1)_{L_g}$ for model 2.

	$SU(3)_C$	$SU(3)_L$	$U(1)_X$	$U(1)_{L_g}$
Q_{nL}	3	$\bar{\mathbf{3}}$	0	$\frac{2}{3}$
Q_{3L}	3	3	$\frac{1}{3}$	$-\frac{2}{3}$
u_{iR}	3	1	$\frac{2}{3}$	0
d_{iR}	3	1	$-\frac{1}{3}$	0
T_R	3	1	$\frac{2}{3}$	-2
B_{nR}	3	1	$-\frac{1}{3}$	2

Table V: Quark assignments under $SU(3)_C \times SU(3)_L \times U(1)_X \times U(1)_{L_g}$ for model 2.

	$SU(3)_C$	$SU(3)_L$	$U(1)_X$	$U(1)_{L_g}$
L_{iL}	1	3	$-\frac{1}{3}$	$\frac{1}{3}$
l_{iR}	1	1	1	-5
E_{iL}	1	1	-1	5
E_{iR}	1	1	-1	1
N_{iR}	1	1	0	-1
Ψ_{nR}	1	1	0	0

Table VI: Lepton assignments under $SU(3)_C \times SU(3)_L \times U(1)_X \times U(1)_{L_g}$ for model 2.

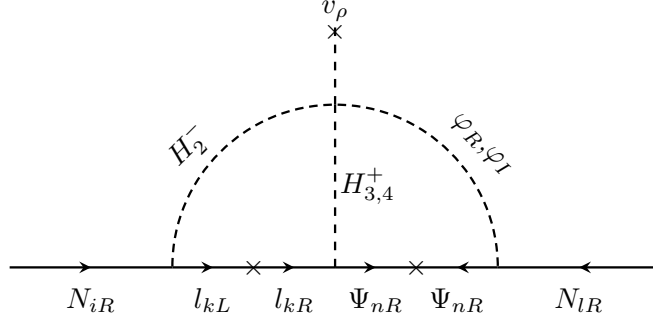


Figure 2: Two-loop Feynman diagram contributing to the Majorana neutrino mass submatrix μ in model 2.

With the above-specified particle content and symmetries, the following Yukawa terms for the quark and lepton sectors arise:

$$\begin{aligned}
 -\mathcal{L}_Y^{(l)} = & \sum_{i=1}^3 \sum_{j=1}^3 (y_E)_{ij} \bar{L}_{iL} \rho E_{jR} + \sum_{i=1}^3 \sum_{j=1}^3 (y_l)_{ij} \bar{E}_{iL} \phi l_{jR} + \sum_{i=1}^3 \sum_{j=1}^3 (x_E)_{ij} \bar{E}_{iL} \sigma E_{jR} \\
 & + \sum_{i=1}^3 \sum_{j=1}^3 (y_N)_{ij} \bar{L}_{iL} \chi N_{jR} + \sum_{i=1}^3 \sum_{j=1}^3 (y_L)_{ij} \varepsilon_{abc} \bar{L}_{iL} (L_{jL}^C)^b (\rho^*)^c
 \end{aligned} \quad (11)$$

$$\begin{aligned}
 & + \sum_{n=1}^2 \sum_{k=1}^2 (y_\Psi)_{nk} \bar{\Psi}_{kR}^C \xi^+ l_{kR} + \sum_{n=1}^2 \sum_{k=1}^2 (x_N)_{nk} \bar{N}_{nR}^C \varphi \Psi_{kR} + \sum_{n=1}^2 \sum_{k=1}^2 (m_\Psi)_{nk} \Psi_{nR} \bar{\Psi}_{kR}^C + H.c
 \end{aligned} \quad (12)$$

$$\begin{aligned}
 -\mathcal{L}_Y^{(q)} = & \sum_{n=1}^2 \sum_{i=1}^3 (y_u)_{ni} \bar{Q}_{nL} \rho^* u_{iR} + \sum_{i=1}^3 (y_u)_{3i} \bar{Q}_{3L} \eta u_{iR} + \sum_{n=1}^2 \sum_{i=1}^3 (y_d)_{ni} \bar{Q}_{nL} \eta^* d_{iR} + \sum_{i=1}^3 (y_d)_{3i} \bar{Q}_{3L} \rho d_{iR} \\
 & + \sum_{n=1}^2 \sum_{k=1}^2 (y_B)_{nk} \bar{Q}_{nL} \chi^* B_{kR} + y_T \bar{Q}_{3L} \chi T_R + H.c
 \end{aligned} \quad (13)$$

The Majorana neutrino mass submatrix μ is generated at two loops as shown in Fig. 2 and takes the form [48, 49]:

$$\mu = \sum_{k=3,4} \frac{\lambda_{\rho\varphi H_2^+ H_k^- v_\rho}}{96\pi^2 m_S^2} \left(y_N \widetilde{M}_l g_k^\dagger m_\Psi^T x_N^T + x_N m_\Psi g_k^* \widetilde{M}_l^T y_N^T \right) J \left(\frac{m_{H_k^-}^2}{m_{H_2^+}^2} \right), \quad (14)$$

in which,

$$\begin{aligned}
 m_S &= \max(m_{H_k^-}, m_{H_2^+}), \\
 J(\varkappa) &= \begin{cases} 1 + \frac{3}{\pi^2} (\ln^2 \varkappa - 1) & \text{for } \varkappa \gg 1 \\ 1 & \text{for } \varkappa \rightarrow 0. \end{cases},
 \end{aligned} \quad (15)$$

and the charged scalar fields H_k^\pm ($k = 3, 4$) are defined by the Eq.(60) with their masses are given by the Eq.(58) while

$$g_3 = y_\Psi \cos \alpha_{3(2)}, \quad g_4 = -y_\Psi \sin \alpha_{3(2)}. \quad (16)$$

III. SCALAR POTENTIAL AND ITS TREE LEVEL STABILITY

In this section, we examine the mass spectra of the scalar fields in detail for the two models discussed above. We divide the analysis into two parts, with each part corresponding to the investigation of one variant.

A. The scalar sector in Model-1

With the scalar particle content provided, one can construct a scalar potential that is invariant under the symmetries of the model as follows:

$$\begin{aligned}
V_1 = & \mu_\chi^2 \chi^\dagger \chi + \mu_\rho^2 \rho^\dagger \rho + \mu_\eta^2 \eta^\dagger \eta + \mu_\sigma^2 \sigma^\dagger \sigma + \mu_\varphi^2 \varphi^\dagger \varphi + \mu_\xi^2 \xi^\dagger \xi + A(\varphi^2 \sigma + h.c) \\
& + \lambda_1 (\chi^\dagger \chi)^2 + \lambda_2 (\eta^\dagger \eta)^2 + \lambda_3 (\rho^\dagger \rho)^2 + \lambda_4 (\sigma^\dagger \sigma)^2 + \lambda_5 (\varphi^\dagger \varphi)^2 + \lambda_6 (\xi^\dagger \xi)^2 \\
& + \lambda_7 (\chi^\dagger \chi)(\eta^\dagger \eta) + \lambda_8 (\chi^\dagger \chi)(\rho^\dagger \rho) + \lambda_9 (\eta^\dagger \eta)(\rho^\dagger \rho) + \lambda_{10} (\chi^\dagger \eta)(\eta^\dagger \chi) + \lambda_{11} (\chi^\dagger \rho)(\rho^\dagger \chi) + \lambda_{12} (\eta^\dagger \rho)(\rho^\dagger \eta) \\
& + \lambda_{13} (\sigma^\dagger \sigma)(\chi^\dagger \chi) + \lambda_{14} (\sigma^\dagger \sigma)(\rho^\dagger \rho) + \lambda_{15} (\sigma^\dagger \sigma)(\eta^\dagger \eta) + \lambda_{16} (\varphi^\dagger \varphi)(\chi^\dagger \chi) + \lambda_{17} (\varphi^\dagger \varphi)(\rho^\dagger \rho) + \lambda_{18} (\varphi^\dagger \varphi)(\eta^\dagger \eta) \\
& + \lambda_{19} (\xi^\dagger \xi)(\chi^\dagger \chi) + \lambda_{20} (\xi^\dagger \xi)(\rho^\dagger \rho) + \lambda_{21} (\xi^\dagger \xi)(\eta^\dagger \eta) + \lambda_{22} (\sigma^\dagger \sigma)(\varphi^\dagger \varphi) + \lambda_{23} (\sigma^\dagger \sigma)(\xi^\dagger \xi) + \lambda_{24} (\varphi^\dagger \varphi)(\xi^\dagger \xi) \\
& + (B \epsilon^{ijk} \eta_i \rho_j \chi_k \xi + H.c).
\end{aligned} \tag{17}$$

After expanding the scalar fields around their VEVs and substituting them into Eq. (17), we can establish the following constraints at the tree level

$$\begin{aligned}
\mu_\chi^2 + \lambda_1 v_\chi^2 + \frac{1}{2} (\lambda_7 v_\eta^2 + \lambda_8 v_\rho^2 + \lambda_{13} v_\sigma^2 + \lambda_{19} v_\xi^2) + B \frac{v_\eta v_\rho v_\xi}{2v_\chi} &= 0, \\
\mu_\eta^2 + \lambda_2 v_\chi^2 + \frac{1}{2} (\lambda_7 v_\chi^2 + \lambda_9 v_\rho^2 + \lambda_{15} v_\sigma^2 + \lambda_{21} v_\xi^2) + B \frac{v_\chi v_\rho v_\xi}{2v_\eta} &= 0, \\
\mu_\rho^2 + \lambda_3 v_\chi^2 + \frac{1}{2} (\lambda_8 v_\chi^2 + \lambda_9 v_\eta^2 + \lambda_{14} v_\sigma^2 + \lambda_{20} v_\xi^2) + B \frac{v_\chi v_\eta v_\xi}{2v_\rho} &= 0, \\
\mu_\sigma^2 + \lambda_4 v_\sigma^2 + \frac{1}{2} (\lambda_{13} v_\chi^2 + \lambda_{14} v_\rho^2 + \lambda_{15} v_\eta^2 + \lambda_{23} v_\xi^2) &= 0, \\
\mu_\xi^2 + \lambda_6 v_\xi^2 + \frac{1}{2} (\lambda_{19} v_\chi^2 + \lambda_{20} v_\rho^2 + \lambda_{21} v_\eta^2 + \lambda_{23} v_\sigma^2) + B \frac{v_\eta v_\rho v_\chi}{2v_\xi} &= 0.
\end{aligned} \tag{18}$$

1. Charged scalar sector

There are four charged scalar fields: ρ_1^- , ρ_3^- , η_2^- , and χ_2^- , which are mixed in pairs: ρ_1^- mixes with η_2^- , and ρ_3^- mixes with χ_2^- . In the basis (ρ_1^-, η_2^-) , the squared mass matrix is:

$$M_{c1(1)}^2 = \frac{\lambda_{12} v_\eta v_\rho - B v_\xi v_\chi}{2} \begin{pmatrix} \frac{v_\eta}{v_\rho} & 1 \\ 1 & \frac{v_\rho}{v_\eta} \end{pmatrix}. \tag{19}$$

Note that here, the subscript (1) stands for model 1 and later when we discuss model 2, we will use the subscript (2). Diagonalizing this matrix, we get one massless field, which is identified to be the Goldstone boson $G_{1(1)}^-$ eaten by $W_{(1)}^-$ boson and one massive boson $H_{1(1)}^-$ with squared mass given by:

$$m_{H_{1(1)}^-}^2 = \frac{(v_\eta^2 + v_\rho^2)}{2v_\eta v_\rho} (\lambda_{12} v_\eta v_\rho - B v_\xi v_\chi). \tag{20}$$

The physical fields are determined as:

$$G_{1(1)}^- = \rho_1^- \cos \alpha_{1(1)} - \eta_2^- \sin \alpha_{1(1)}, \tag{21}$$

$$H_{1(1)}^- = \rho_1^- \sin \alpha_{1(1)} + \eta_2^- \cos \alpha_{1(1)} \tag{22}$$

where the mixing angle is given by the relation:

$$\tan \alpha_{1(1)} = -\frac{v_\eta}{v_\rho}. \tag{23}$$

Ensuring the value of $m_{H_{1(1)}^-}^2$ to be positive puts a constraint on the parameter B as:

$$B < \frac{\lambda_{12} v_\eta v_\rho}{v_\xi v_\chi}. \tag{24}$$

In the basis (ρ_3^-, χ_2^-) , the squared mass matrix is:

$$M_{c2(1)}^2 = \frac{\lambda_{11} v_\chi v_\rho - B v_\xi v_\eta}{2} \begin{pmatrix} \frac{v_\chi}{v_\rho} & 1 \\ 1 & \frac{v_\rho}{v_\chi} \end{pmatrix}. \quad (25)$$

The physical states are:

$$G_{2(1)}^- = \rho_3^- \cos \alpha_{2(1)} - \chi_2^- \sin \alpha_{2(1)}, \quad (26)$$

$$H_{2(1)}^- = \rho_3^- \sin \alpha_{2(1)} + \chi_2^- \cos \alpha_{2(1)}, \quad (27)$$

with the mixing angle $\alpha_{2(1)}$ is determined by

$$\tan \alpha_{2(1)} = -\frac{v_\rho}{v_\chi}. \quad (28)$$

After diagonalizing, the mass-squared matrix has the form given below:

$$M_{c2(1)}^{2diag} = \frac{\lambda_{11} v_\chi v_\rho - B v_\xi v_\eta}{2} \begin{pmatrix} 0 & 0 \\ 0 & \frac{v_\rho^2 + v_\chi^2}{v_\rho v_\chi} \end{pmatrix}, \quad (29)$$

The massless Goldstone boson $G_{2(1)}^-$ is eaten by $Y_{(1)}^-$ boson whereas the mass of $H_{2(1)}^-$ is given by the non-zero eigenvalue of the matrix. Again, requiring the expression for the mass-squared of the field $H_{2(1)}^-$ to be positive puts a constraint on the parameter B as:

$$B < \frac{\lambda_{11} v_\chi v_\rho}{v_\xi v_\eta}, \quad (30)$$

2. CP odd scalar sector

The model contains seven CP-odd scalar fields: $I_\sigma, I_\varphi, I_\chi^1, I_\chi^3, I_\rho, I_\eta^1, I_\eta^3$. Two of these, I_φ and I_σ , are completely decoupled. These themselves correspond to the physical states. The $I_{\sigma(1)}$ field is massless whereas the squared mass of the field $I_{\varphi(1)}$ is given as:

$$m_{I_{\varphi(1)}}^2 = \sqrt{2} A v_\sigma + \mu_\varphi^2 + \frac{1}{2} (\lambda_{16} v_\chi^2 + \lambda_{17} v_\rho^2 + \lambda_{18} v_\eta^2 + \lambda_{22} v_\sigma^2 + \lambda_{24} v_\xi^2). \quad (31)$$

The mass in Eq.(31) gives the contribution to the neutrino submatrix μ as mentioned in the subsection II A. The field $I_{\sigma(1)}$ can be identified as the Majoron, which is the Goldstone boson associated with the spontaneous breaking of the $U(1)_{L_g}$ global lepton number symmetry. Despite being massless, this Goldstone is phenomenologically harmless since it is a gauge singlet. The Majoron can acquire a mass from a soft-breaking mass term in the scalar sector.

The five fields left are mixed in two groups: $(I_\chi^3, I_\rho, I_\eta^1)$ and (I_χ^1, I_η^3) . Note that I_χ^3, I_ρ and I_η^1 are the components of the scalar representations whose VEVs are non-zero while I_χ^1 and I_η^3 are the components of the scalar representations with vanishing VEVs.

In the basis $(I_\chi^3, I_\rho, I_\eta^1)$, the symmetric mass-squared matrix takes the following form:

$$M_{odd1(1)}^2 = -\frac{B v_\xi}{2} \begin{pmatrix} \frac{v_\eta v_\rho}{v_\chi} & v_\eta & v_\rho \\ & \frac{v_\eta v_\chi}{v_\rho} & v_\chi \\ & & \frac{v_\rho v_\chi}{v_\eta} \end{pmatrix}. \quad (32)$$

Applying the Euler method as used in [50], the diagonalized matrix $M_{odd1(1)}^{2diag}$ takes the following form:

$$M_{odd1(1)}^{2diag} = -\frac{B v_\xi}{2} \begin{pmatrix} 0 & 0 & 0 \\ 0 & 0 & 0 \\ 0 & 0 & \frac{v_\rho v_\chi}{v_\eta} + \frac{v_\chi v_\eta}{v_\rho} + \frac{v_\eta v_\rho}{v_\chi} \end{pmatrix}. \quad (33)$$

From Eq. (33), we see that the model has two massless Goldstone bosons $G_{Z'_{(1)}}, G_{Z_{(1)}}$ and a massive field $A_{1_{(1)}}$ whose mass is given by the non-zero eigenvalue of the matrix $M_{odd1_{(1)}}^2$. The physical states $(G_{Z'_{(1)}}, G_{Z_{(1)}}, A_{1_{(1)}})$ are related to the $(I_\chi^3, I_\rho, I_\eta^1)$ states as below:

$$\begin{pmatrix} G_{Z'_{(1)}} \\ G_{Z_{(1)}} \\ A_{1_{(1)}} \end{pmatrix} = \begin{pmatrix} -\cos \alpha_{3_{(1)}} & -\sin \alpha_{1_{(1)}} \sin \alpha_{3_{(1)}} & \sin \alpha_{1_{(1)}} \cos \alpha_{3_{(1)}} \\ 0 & \cos \alpha_{1_{(1)}} & \sin \alpha_{1_{(1)}} \\ \sin \alpha_{3_{(1)}} & -\sin \alpha_{1_{(1)}} \cos \alpha_{3_{(1)}} & \cos \alpha_{1_{(1)}} \cos \alpha_{3_{(1)}} \end{pmatrix} \begin{pmatrix} I_\chi^3 \\ I_\rho \\ I_\eta^1 \end{pmatrix}, \quad (34)$$

where the third mixing angle is defined by:

$$\tan \alpha_{3_{(1)}} = -\frac{v_\eta}{v_\chi \sqrt{1 + \frac{v_\eta^2}{v_\rho^2}}} = -\frac{v_\eta}{v_\chi} |\cos \alpha_{1_{(1)}}|. \quad (35)$$

In the basis (I_χ^1, I_η^3) , the mass-squared matrix is:

$$M_{odd2_{(1)}}^2 = \frac{(Bv_\xi v_\rho - \lambda_{10} v_\eta v_\chi)}{2} \begin{pmatrix} \frac{v_\eta}{v_\chi} & 1 \\ 1 & \frac{v_\chi}{v_\eta} \end{pmatrix}. \quad (36)$$

In the mass basis, the matrix $M_{odd2_{(1)}}^2$ has the following form:

$$M_{odd2_{(1)}}^{2diag} = \frac{(Bv_\xi v_\rho - \lambda_{10} v_\eta v_\chi)}{2} \begin{pmatrix} 0 & 0 \\ 0 & \frac{(v_\eta^2 + v_\chi^2)}{v_\eta v_\chi} \end{pmatrix}. \quad (37)$$

Thus, the mixing of I_χ^1 and I_η^3 provides one massless field, $G_{X_{(1)}}^\Im$, which is identified as the imaginary component of the Goldstone boson $G_{X_{(1)}}^0$ eaten by the bilepton gauge boson $X_{(1)}^0$, and one massive field, denoted as $A_{2_{(1)}}$. The physical fields are presented as follows:

$$G_{X_{(1)}}^\Im = I_\chi^1 \cos \alpha_{4_{(1)}} - I_\eta^3 \sin \alpha_{4_{(1)}}, \quad A_{2_{(1)}} = I_\chi^1 \sin \alpha_{4_{(1)}} + I_\eta^3 \cos \alpha_{4_{(1)}}.$$

The mixing angle is defined as

$$\tan \alpha_{4_{(1)}} = \frac{v_\eta}{v_\chi}. \quad (38)$$

Thus, the CP odd sector consists of four massless fields $(G_{Z_{(1)}}, G_{Z'_{(1)}}, G_{X_{(1)}}^\Im, I_{\sigma_{(1)}})$ and three massive fields $(A_{1_{(1)}}, A_{2_{(1)}} \text{ and } I_{\varphi_{(1)}})$. The masses of the A_1, A_2 fields should be of the same scale as that of v_χ .

3. CP-even scalar sector

The model consists of eight CP-even scalar fields: $R_\varphi, R_\sigma, R_\chi^1, R_\chi^3, R_\xi, R_\rho, R_\eta^1, R_\eta^3$. Five of them $(R_\sigma, R_\chi^3, R_\xi, R_\rho, R_\eta^1)$ with non-zero VEVs mix among themselves. The remaining three acquire no VEVs. but only R_χ^1, R_η^3 mix with each other. The remaining scalar R_φ does not mix with any other scalars and its mass is given as:

$$m_{R_{\varphi_{(1)}}}^2 = m_{I_{\varphi_{(1)}}}^2. \quad (39)$$

Thus R_φ corresponds to the gauge eigenstate as well as the mass eigenstate, just like I_φ . The masses of $R_{\varphi_{(1)}}$ and $I_{\varphi_{(1)}}$ are the same and should be at the v_χ scale. Thus, they can combine to form a complex scalar field with a mass also depending on the parameter A which is the coefficient of the $\varphi^2 \sigma$ term in the potential V_1 .

In the basis (R_χ^1, R_η^3) , the mass mixing matrix $M_{even1_{(1)}}^2$ is as same as the matrix $M_{odd2_{(1)}}^2$ in Eq. (37). One obtains $G_{X_{(1)}}^\Re$ corresponding to the real component of the Goldstone boson $G_{X_{(1)}}^0$, which is absorbed by the gauge boson $X_{(1)}^0$,

and a massive boson $\mathcal{H}_{R(1)}$ with mass $m_{\mathcal{H}_{R(1)}}^2 = m_{A_{2(1)}}^2$. The mixing angle to define the physical fields is also $\alpha_{4(1)}$ as in the Eq.(38).

The mass-squared matrix corresponding to the remaining five CP-even scalars $(R_\sigma, R_\chi^3, R_\xi, R_\rho, R_\eta^1)$ is given as follows:

$$M_{even2(1)}^2 = \begin{pmatrix} 2\lambda_4 v_\sigma^2 & \lambda_{13} v_\sigma v_\chi & \lambda_{23} v_\xi v_\sigma & \lambda_{14} v_\rho v_\sigma & \lambda_{15} v_\eta v_\sigma \\ 2\lambda_1 v_\chi^2 - \frac{Bv_\eta v_\xi v_\rho}{2v_\chi} & \frac{Bv_\eta v_\rho}{2} + \lambda_{19} v_\xi v_\chi & \frac{Bv_\eta v_\xi}{2} + \lambda_8 v_\rho v_\chi & \frac{Bv_\xi v_\rho}{2} + \lambda_7 v_\eta v_\chi & \\ & 2\lambda_6 v_\xi^2 - \frac{Bv_\eta v_\rho v_\chi}{2v_\xi} & \frac{Bv_\eta v_\chi}{2} + \lambda_{20} v_\xi v_\rho & \frac{Bv_\rho v_\chi}{2} + \lambda_{21} v_\eta v_\xi & \\ & & 2\lambda_3 v_\rho^2 - \frac{Bv_\eta v_\xi v_\chi}{2v_\rho} & \frac{Bv_\xi v_\chi}{2} + \lambda_9 v_\eta v_\rho & \\ & & & 2\lambda_2 v_\eta^2 - \frac{Bv_\xi v_\rho v_\chi}{2v_\eta} & \end{pmatrix}. \quad (40)$$

We assume that $v_\sigma, v_\chi \gg v_\xi, v_\eta, v_\rho$. Due to this assumption, the matrix $M_{even2(1)}^2$ can be separated into two blocks corresponding to the two bases (R_σ, R_χ^3) and $(R_\xi, R_\rho, R_\eta^1)$. The first block with two components has larger VEVs, while the second one has smaller VEVs (\sim EW scale).

In the basis (R_σ, R_χ^3) , the squared mass matrix has the form:

$$M_{even2a(1)}^2 = \begin{pmatrix} 2\lambda_4 v_\sigma^2 & \lambda_{13} v_\sigma v_\chi \\ \lambda_{13} v_\sigma v_\chi & 2\lambda_1 v_\chi^2 - \frac{Bv_\eta v_\xi v_\rho}{2v_\chi} \end{pmatrix}. \quad (41)$$

The matrix $M_{even2a(1)}^2$ provides two heavy massive physical fields $\mathcal{H}_{1(1)}, \mathcal{H}_{2(1)}$, which are related to the gauge eigenstates (R_σ, R_χ^3) as follows:

$$\begin{pmatrix} \mathcal{H}_{1(1)} \\ \mathcal{H}_{2(1)} \end{pmatrix} = \begin{pmatrix} \cos \beta_{1(1)} & \sin \beta_{1(1)} \\ -\sin \beta_{1(1)} & \cos \beta_{1(1)} \end{pmatrix} \begin{pmatrix} R_\sigma \\ R_\chi^3 \end{pmatrix}, \quad (42)$$

with the mixing angle defined by:

$$\tan 2\beta_{1(1)} = \frac{4\lambda_{13} v_\sigma v_\chi^2}{Bv_\xi v_\eta v_\rho + 4\lambda_4 v_\sigma^2 v_\chi - 4\lambda_1 v_\chi^3}. \quad (43)$$

The squared masses of the two scalars $\mathcal{H}_{1(1)}$ and $\mathcal{H}_{2(1)}$ are:

$$m_{\mathcal{H}_{1,2(1)}}^2 = \lambda_1 v_\chi^2 + \lambda_4 v_\sigma^2 - \frac{Bv_\eta v_\rho v_\xi}{4v_\chi} \pm \sqrt{\lambda_{13}^2 v_\chi^2 v_\sigma^2 + \left(\frac{Bv_\eta v_\rho v_\xi}{4v_\chi} + \lambda_4 v_\sigma^2 - \lambda_1 v_\chi^2 \right)^2}. \quad (44)$$

In the basis $(R_\xi, R_\rho, R_\eta^1)$, the mass-squared matrix is:

$$M_{even2b(1)}^2 = \begin{pmatrix} 2\lambda_6 v_\xi^2 - \frac{Bv_\eta v_\rho v_\chi}{2v_\xi} & \frac{Bv_\eta v_\chi}{2} + \lambda_{20} v_\xi v_\rho & \frac{Bv_\rho v_\chi}{2} + \lambda_{21} v_\eta v_\xi \\ & 2\lambda_3 v_\rho^2 - \frac{Bv_\eta v_\xi v_\chi}{2v_\rho} & \frac{Bv_\xi v_\chi}{2} + \lambda_9 v_\eta v_\rho \\ & & 2\lambda_2 v_\eta^2 - \frac{Bv_\xi v_\rho v_\chi}{2v_\eta} \end{pmatrix} \quad (45)$$

In the usual scenario, the physical states will be connected to the gauge eigenstates by a 3×3 unitary matrix (see Appendix.B for details) as below:

$$\begin{pmatrix} \mathcal{H}_{3(1)} \\ h_{(1)} \\ \mathcal{H}_{4(1)} \end{pmatrix} \simeq \begin{pmatrix} \cos \beta_{3(1)} & \sin \beta_{2(1)} \sin \beta_{3(1)} & -\cos \beta_{2(1)} \sin \beta_{3(1)} \\ -\sin \beta_{3(1)} & \sin \beta_{2(1)} \cos \beta_{3(1)} & -\cos \beta_{2(1)} \cos \beta_{3(1)} \\ 0 & \cos \beta_{2(1)} & \sin \beta_{2(1)} \end{pmatrix} \begin{pmatrix} R_\xi \\ R_\rho \\ R_\eta^1 \end{pmatrix}. \quad (46)$$

Then, the particle h corresponds to the SM Higgs-like boson and its squared mass is given by:

$$m_{h(1)}^2 = \frac{-Bv_\chi v_\xi}{2} \left(\frac{v_\rho}{v_\eta} + \frac{v_\eta}{v_\rho} \right) = \frac{-Bv_\chi v_\xi v^2}{2v_\rho v_\eta}, \quad (47)$$

where $v^2 = v_\rho^2 + v_\eta^2 = 246^2 \text{ GeV}^2$ and the parameter B should be negative with the absolute value of Bv_χ being in the EW scale like v_ξ, v_ρ and v_η . Masses of the two other scalars, $\mathcal{H}_{3,4(1)}$ are:

$$m_{\mathcal{H}_{3,4(1)}}^2 = -\frac{Bv_\chi v_\rho v_\eta}{4vv_\xi} \left(\sqrt{v^2 + 16v_\xi^2} \pm v \right). \quad (48)$$

Since Bv_χ is at the EW scale, the $\mathcal{H}_{4(1)}$ boson could potentially be the light Higgs boson as announced by the CMS collaboration [51]. On the other hand, the scalar $\mathcal{H}_{3(1)}$ can have a mass at the TeV or subTeV scale.

B. The scalar sector in Model-2

From the particle spectrum defined in Sec. II, the gauge invariant scalar potential for model 2 with two-loop inverse seesaw mechanism is given as:

$$\begin{aligned} V_2 = & \mu_\chi^2 \chi^\dagger \chi + \mu_\rho^2 \rho^\dagger \rho + \mu_\eta^2 \eta^\dagger \eta + \mu_\sigma^2 \sigma^\dagger \sigma + \mu_\varphi^2 \varphi^\dagger \varphi + \mu_\zeta^2 \zeta^+ \zeta^- + \mu_\xi^2 \xi^+ \xi^- + \mu_\phi^2 \phi^* \phi + (f \varepsilon^{ijk} \eta_i \rho_j \chi_k + H.c) \\ & + \lambda_1 (\chi^\dagger \chi)^2 + \lambda_2 (\eta^\dagger \eta)^2 + \lambda_3 (\rho^\dagger \rho)^2 + \lambda_4 (\sigma^\dagger \sigma)^2 + \lambda_5 (\varphi^\dagger \varphi)^2 + \lambda_6 (\zeta^+ \zeta^-)^2 + \lambda_7 (\xi^+ \xi^-)^2 \\ & + \lambda_8 (\chi^\dagger \chi)(\eta^\dagger \eta) + \lambda_9 (\chi^\dagger \chi)(\rho^\dagger \rho) + \lambda_{10} (\eta^\dagger \eta)(\rho^\dagger \rho) + \lambda_{11} (\chi^\dagger \chi)(\eta^\dagger \eta) + \lambda_{12} (\chi^\dagger \rho)(\rho^\dagger \chi) + \lambda_{13} (\eta^\dagger \rho)(\rho^\dagger \eta) \\ & + \lambda_{14} (\sigma^\dagger \sigma)(\chi^\dagger \chi) + \lambda_{15} (\sigma^\dagger \sigma)(\rho^\dagger \rho) + \lambda_{16} (\sigma^\dagger \sigma)(\eta^\dagger \eta) + \lambda_{17} (\varphi^\dagger \varphi)(\chi^\dagger \chi) + \lambda_{18} (\varphi^\dagger \varphi)(\rho^\dagger \rho) + \lambda_{19} (\varphi^\dagger \varphi)(\eta^\dagger \eta) \\ & + \lambda_{20} (\sigma^\dagger \sigma)(\varphi^\dagger \varphi) + \lambda_{21} (\sigma^\dagger \sigma)(\zeta^+ \zeta^-) + \lambda_{22} (\zeta^+ \zeta^-)(\chi^\dagger \chi) + \lambda_{23} (\zeta^+ \zeta^-)(\rho^\dagger \rho) + \lambda_{24} (\zeta^+ \zeta^-)(\eta^\dagger \eta) + \lambda_{25} (\varphi^\dagger \varphi)(\zeta^+ \zeta^-) \\ & + \lambda_{26} (\sigma^\dagger \sigma)(\xi^+ \xi^-) + \lambda_{27} (\xi^+ \xi^-)(\chi^\dagger \chi) + \lambda_{28} (\xi^+ \xi^-)(\rho^\dagger \rho) + \lambda_{29} (\xi^+ \xi^-)(\eta^\dagger \eta) + \lambda_{30} (\varphi^\dagger \varphi)(\xi^+ \xi^-) \\ & + \lambda_{31} (\chi^\dagger \rho \zeta^- \varphi^* + H.c) + \lambda_{32} (\zeta^+ \xi^- \sigma^2 + H.c) + \lambda_{33} (\zeta^+ \zeta^-)(\xi^+ \xi^-) + \lambda_{34} [(\chi^\dagger \eta) \varphi^2 + H.c] \\ & + \lambda_{35} (\phi^* \phi)^2 + \lambda_{36} (\phi^* \phi)(\chi^\dagger \chi) + \lambda_{37} (\phi^* \phi)(\eta^\dagger \eta) + \lambda_{38} (\phi^* \phi)(\rho^\dagger \rho) + \lambda_{39} (\phi^* \phi)(\sigma^\dagger \sigma) \\ & + \lambda_{40} (\phi^* \phi)(\varphi^\dagger \varphi) + \lambda_{41} (\phi^* \phi)(\zeta^+ \zeta^-) + \lambda_{42} (\phi^* \phi)(\xi^+ \xi^-). \end{aligned} \quad (49)$$

Expanding the scalar fields around their VEVs and substituting into Eq.(49), we obtain the following constraints at tree level:

$$\begin{aligned} \mu_\chi^2 + \lambda_1 v_\chi^2 + \frac{1}{2} (\lambda_8 v_\eta^2 + \lambda_9 v_\rho^2 + \lambda_{14} v_\sigma^2 + \lambda_{36} v_\phi^2) + f \frac{v_\eta v_\rho}{\sqrt{2} v_\chi} &= 0, \\ \mu_\eta^2 + \lambda_2 v_\eta^2 + \frac{1}{2} (\lambda_8 v_\chi^2 + \lambda_{10} v_\rho^2 + \lambda_{16} v_\sigma^2 + \lambda_{37} v_\phi^2) + f \frac{v_\eta v_\rho}{\sqrt{2} v_\eta} &= 0, \\ \mu_\rho^2 + \lambda_3 v_\rho^2 + \frac{1}{2} (\lambda_9 v_\chi^2 + \lambda_{10} v_\eta^2 + \lambda_{15} v_\sigma^2 + \lambda_{38} v_\phi^2) + f \frac{v_\eta v_\rho}{\sqrt{2} v_\chi} &= 0, \\ \mu_\sigma^2 + \lambda_4 v_\sigma^2 + \frac{1}{2} (\lambda_{14} v_\chi^2 + \lambda_{15} v_\rho^2 + \lambda_{16} v_\eta^2 + \lambda_{39} v_\phi^2) &= 0, \\ \mu_\phi^2 + \lambda_{35} v_\phi^2 + \frac{1}{2} (\lambda_{36} v_\chi^2 + \lambda_{37} v_\eta^2 + \lambda_{38} v_\rho^2 + \lambda_{39} v_\sigma^2) &= 0. \end{aligned} \quad (50)$$

1. Charged scalar sector

There are six charged scalar fields in this variant of the 3-3-1 model. They are: $\rho_1^-, \rho_3^-, \eta_2^-, \chi_2^-, \xi^-,$ and ζ^- , and they mix in pairs. ρ_1^- mixes with η_2^- , ρ_3^- mixes with χ_2^- , and ξ^- mixes with ζ^- . In the basis (ρ_1^-, η_2^-) , the squared mass matrix has the form:

$$M_{c1(2)}^2 = \frac{\lambda_{13} v_\eta v_\rho - \sqrt{2} f v_\chi}{2} \begin{pmatrix} \frac{v_\eta}{v_\rho} & 1 \\ 1 & \frac{v_\rho}{v_\eta} \end{pmatrix}. \quad (51)$$

Diagonalizing the matrix $M_{c1(2)}^2$ gives the physical states as the massless Goldstone boson $G_{1(2)}^- = \rho_1^- \cos \alpha_{1(2)} + \eta_2^- \sin \alpha_{1(2)}$ eaten by the longitudinal components of the $W_{(2)}^-$ boson and the massive charged scalar $H_{1(2)}^- = -\rho_1^- \sin \alpha_{1(2)} + \eta_2^- \cos \alpha_{1(2)}$ with mass given by:

$$m_{H_{1(2)}^-}^2 = \frac{v^2}{2v_\eta v_\rho} \left(\lambda_{13} v_\eta v_\rho - \sqrt{2} f v_\chi \right), \quad (52)$$

and the mixing angle $\alpha_{1(2)} = \alpha_{1(1)}$ is the same as the one defined in the Eq.(23).

The requirement of the mass-squared to be positive in Eq.(52) puts the following constraint on the parameter f :

$$f < \frac{\lambda_{13}v_\eta v_\rho}{\sqrt{2}v_\chi}. \quad (53)$$

In the basis (ρ_3^-, χ_2^-) , the squared mass matrix is:

$$M_{c2(2)}^2 = \frac{\lambda_{12}v_\chi v_\rho - \sqrt{2}f v_\eta}{2} \begin{pmatrix} \frac{v_\chi}{v_\rho} & 1 \\ 1 & \frac{v_\rho}{v_\chi} \end{pmatrix}. \quad (54)$$

After diagonalization, we obtain a massless Goldstone boson, $G_{2(2)}^-$, which is absorbed by the $Y_{(2)}^-$ bilepton gauge boson, and a massive field, $H_{2(2)}^-$, with mass given by:

$$m_{H_{2(2)}^-}^2 = \frac{(v_\chi^2 + v_\rho^2)}{2v_\rho v_\chi} \left(\lambda_{12}v_\rho v_\chi - \sqrt{2}f v_\eta \right), \quad (55)$$

where the mixing angle is $\alpha_{2(2)} = \alpha_{2(1)}$ is the same as the one in defined in Eq.(28). Again, requiring the expression for the mass-squared defined in Eq.(55) to be greater than 0, we obtain the following restriction on f :

$$f < \lambda_{12} \frac{v_\chi v_\rho}{\sqrt{2}v_\eta}. \quad (56)$$

In the basis (ξ^-, ζ^-) , the squared mass matrix is:

$$M_{c3(2)}^2 = \frac{1}{2} \begin{pmatrix} 2\mu_\xi^2 + \lambda_{26}v_\sigma^2 + \lambda_{27}v_\chi^2 + \lambda_{28}v_\rho^2 + \lambda_{29}v_\eta^2 + \lambda_{42}v_\phi^2 & \lambda_{32}v_\sigma^2 \\ \lambda_{32}v_\sigma^2 & 2\mu_\zeta^2 + \lambda_{21}v_\sigma^2 + \lambda_{22}v_\chi^2 + \lambda_{23}v_\rho^2 + \lambda_{24}v_\eta^2 + \lambda_{41}v_\phi^2 \end{pmatrix}. \quad (57)$$

We can consistently consider a simplified benchmark scenario where $\lambda_{21} = \lambda_{26}$, $\lambda_{22} = \lambda_{27}$, $\lambda_{23} = \lambda_{28}$, $\lambda_{24} = \lambda_{29}$, $\lambda_{41} = \lambda_{42}$. Then we get two massive fields with masses:

$$m_{H_{3,4(2)}^-} = \frac{1}{2} \left(\mu_\zeta^2 + \mu_\xi^2 + \lambda_{26}v_\sigma^2 + \lambda_{27}v_\chi^2 + \lambda_{28}v_\rho^2 + \lambda_{29}v_\eta^2 + \lambda_{42}v_\phi^2 \pm \sqrt{(\mu_\zeta^2 - \mu_\xi^2)^2 + \lambda_{32}^2 v_\sigma^4} \right). \quad (58)$$

In this case, the mixing angle $\alpha_{3(2)}$ is defined by:

$$\tan \alpha_{3(2)} = - \frac{\sqrt{\left(\sqrt{(\mu_\zeta^2 - \mu_\xi^2)^2 + \lambda_{32}^2 v_\sigma^4} + \mu_\xi^2 - \mu_\zeta^2 \right)^2 + \lambda_{32}^2 v_\sigma^4}}{\sqrt{2} \sqrt{\mu_\zeta^2 - \mu_\xi^2 + \sqrt{(\mu_\zeta^2 - \mu_\xi^2)^2 + \lambda_{32}^2 v_\sigma^4}} \left((\mu_\zeta^2 - \mu_\xi^2)^2 + \lambda_{32}^2 v_\sigma^4 \right)^{\frac{1}{4}}}. \quad (59)$$

Then the physical states of these two charged scalar fields are given as:

$$\begin{aligned} H_{3(2)}^- &= \xi^\pm \cos \alpha_{3(2)} + \zeta^\pm \sin \alpha_{3(2)}, \\ H_{4(2)}^- &= -\xi^\pm \sin \alpha_{3(2)} + \zeta^\pm \cos \alpha_{3(2)}. \end{aligned} \quad (60)$$

These two charged Higgs give contribution to the Majorana neutrino mass submatrix μ as shown in the Fig.2.

2. CP-odd scalar sector

The model consists of eight CP-odd scalar fields: $I_\varphi, I_\phi, I_\sigma, I_\chi^1, I_\chi^3, I_\rho, I_\eta^1, I_\eta^3$. The fields I_ϕ and I_σ do not mix with other fields. The I_σ can be identified with the Majoron, as in the model 1. The I_φ corresponds to a massive physical field with the mass:

$$m_{I_{\varphi(2)}}^2 = \frac{1}{2} (2\mu_\varphi^2 + \lambda_{19}v_\eta^2 + \lambda_{18}v_\rho^2 + \lambda_{20}v_\sigma^2 + \lambda_{17}v_\chi^2 + \lambda_{40}v_\phi^2). \quad (61)$$

The five remaining fields, $I_\chi^1, I_\chi^3, I_\rho, I_\eta^1, I_\eta^3$, mix in two groups: $(I_\chi^3, I_\rho, I_\eta^1)$ and (I_χ^1, I_η^3) . In the basis $(I_\chi^3, I_\rho, I_\eta^1)$, the squared mass matrix for the electrically neutral CP-odd scalars takes the form:

$$M_{odd1(2)}^2 = -\frac{f}{\sqrt{2}} \begin{pmatrix} \frac{v_\eta v_\rho}{v_\chi} & v_\eta & v_\rho \\ & \frac{v_\eta v_\chi}{v_\rho} & v_\chi \\ & & \frac{v_\rho v_\chi}{v_\eta} \end{pmatrix}. \quad (62)$$

The matrix in the Eq.(62) can be diagonalized by the 3×3 matrix:

$$U_{odd1(2)} = \begin{pmatrix} -\cos \alpha_{4(2)} & -\sin \alpha_{1(2)} \sin \alpha_{4(2)} & \sin \alpha_{1(2)} \cos \alpha_{4(2)} \\ 0 & \cos \alpha_{1(2)} & \sin \alpha_{1(2)} \\ \sin \alpha_{4(2)} & -\sin \alpha_{1(2)} \cos \alpha_{4(2)} & \cos \alpha_{1(2)} \cos \alpha_{4(2)} \end{pmatrix}, \quad (63)$$

where the mixing angles are defined by:

$$\tan \alpha_{1(2)} = \tan \alpha_{1(1)}, \quad \tan \alpha_{4(2)} = \tan \alpha_{3(1)}. \quad (64)$$

After diagonalizing, the matrix $M_{odd1(2)}^2$ in the Eq.(62) has form:

$$M_{odd1(2)diag}^2 = -\frac{f}{\sqrt{2}} \begin{pmatrix} 0 & 0 & 0 \\ 0 & 0 & 0 \\ 0 & 0 & \frac{v_\rho v_\chi}{v_\eta} + \frac{v_\chi v_\eta}{v_\rho} + \frac{v_\eta v_\rho}{v_\chi} \end{pmatrix} \quad (65)$$

Thus, we obtain two massless physical states, namely the Goldstone bosons $G_{Z(2)}$ and $G_{Z'(2)}$, which are absorbed by the longitudinal components of the Z and Z' gauge bosons, respectively. In addition, there is a massive pseudoscalar with a mass-squared given by $-\frac{f}{\sqrt{2}} \left(\frac{v_\rho v_\chi}{v_\eta} + \frac{v_\chi v_\eta}{v_\rho} + \frac{v_\eta v_\rho}{v_\chi} \right)$. Since this expression has to be positive, the parameter f should always be negative.

In the basis (I_χ^1, I_η^3) , the squared mass matrix for these two electrically neutral CP odd scalars has the form:

$$M_{odd2(2)}^2 = \frac{(-\sqrt{2}f v_\rho + \lambda_{11} v_\eta v_\chi)}{2} \begin{pmatrix} \frac{v_\eta}{v_\chi} & 1 \\ 1 & \frac{v_\chi}{v_\eta} \end{pmatrix}. \quad (66)$$

The matrix $M_{odd2(2)}^2$ in Eq.(66) is diagonalized by the 2×2 matrix:

$$U_{odd2(2)} = \begin{pmatrix} \cos \alpha_{5(2)} & \sin \alpha_{5(2)} \\ -\sin \alpha_{5(2)} & \cos \alpha_{5(2)} \end{pmatrix}, \quad (67)$$

in which,

$$\tan \alpha_{5(2)} = \frac{v_\eta}{v_\chi} = \tan \alpha_{4(1)}. \quad (68)$$

Thus, we get one massless physical field $G_{X(2)}^{\Im}$, which can be identified as the imaginary component of the Goldstone boson $G_{X(2)}^0$. Another physical field is a massive field, $A_{2(2)}$, with squared mass given as $m_{A_{2(2)}}^2 = \frac{(v_\eta^2 + v_\chi^2)}{2v_\eta v_\chi} (\lambda_{11} v_\eta v_\chi - \sqrt{2}f v_\rho)$. Requiring this to be positive, we get the following constraint on the f parameter:

$$f < \lambda_{11} \frac{v_\eta v_\chi}{\sqrt{2}v_\rho}. \quad (69)$$

3. CP even scalar sector

The CP even scalar sector has eight scalar fields: $R_\varphi, R_\sigma, R_\chi^1, R_\chi^3, R_\phi, R_\rho, R_\eta^1, R_\eta^3$. The field R_φ does not mix with the other fields and its mass is given as:

$$m_{R_{\varphi(2)}}^2 = \frac{1}{2} (2\mu\varphi^2 + \lambda_{19}v_\eta^2 + \lambda_{18}v_\rho^2 + \lambda_{20}v_\sigma^2 + \lambda_{17}v_\chi^2 + \lambda_{40}v_\phi^2) = m_{I_{\varphi(2)}}^2. \quad (70)$$

The remaining seven fields left mix in two groups: $(R_\sigma, R_\chi^3, R_\xi, R_\rho, R_\eta^1)$ that acquire non-zero values of VEV and (R_χ^1, R_η^3) with zero VEV. In the basis (R_χ^1, R_η^3) , the mass squared matrix $M_{even_{2(2)}}^2$ has the same form as the matrix $M_{odd_{1(2)}}^2$ given in Eq.(66). Thus, we get the massless field $G_{X(2)}^{\mathfrak{R}^0}$ which can be identified to be the real component of the Goldstone boson which is eaten by the gauge boson $X_{(2)}^0$ and a massive boson $\mathcal{H}_{R(2)}$ with mass $m_{\mathcal{H}_{R(2)}}^2 = m_{A_{2(2)}}^2$. Note that the mixing angle that relates the physical fields to the gauge eigenstates in this case is the same as $\alpha_{5(2)}$ defined in Eq.(68).

In the basis $(R_\sigma, R_\chi^3, R_\phi, R_\rho, R_\eta^1)$, the squared mass matrix for these five electrically neutral CP even scalars has the form:

$$M_{even_{2(2)}}^2 = \begin{pmatrix} 2\lambda_4 v_\sigma^2 & \lambda_{14} v_\sigma v_\chi & \lambda_{39} v_\sigma v_\phi & \lambda_{15} v_\rho v_\sigma & \lambda_{16} v_\eta v_\sigma \\ & 2\lambda_1 v_\chi^2 - \frac{f v_\eta v_\rho}{\sqrt{2} v_\chi} & \lambda_{36} v_\chi v_\phi & \frac{f v_\eta}{\sqrt{2}} + \lambda_9 v_\rho v_\chi & \frac{f v_\rho}{\sqrt{2}} + \lambda_8 v_\eta v_\chi \\ & & 2\lambda_{35} v_\phi^2 & \lambda_{38} v_\rho v_\phi & \lambda_{37} v_\eta v_\phi \\ & & & 2\lambda_3 v_\rho^2 - \frac{f v_\eta v_\chi}{\sqrt{2} v_\rho} & \frac{f v_\chi}{\sqrt{2}} + \lambda_{10} v_\eta v_\rho \\ & & & & 2\lambda_2 v_\eta^2 - \frac{f v_\rho v_\chi}{\sqrt{2} v_\eta} \end{pmatrix}. \quad (71)$$

We assume that their VEVs follow the hierarchy $v_\chi, v_\sigma \gg v_\phi, v_\eta, v_\rho$. Hence, the matrix $M_{even_{1(2)}}^2$ can be separated into two blocks : the first block with higher VEVs and the second one with lower VEVs (\sim EW scale).

In the basis (R_σ, R_χ^3) , the squared mass matrix has the following form:

$$M_{even_{2a(2)}}^2 = \begin{pmatrix} 2\lambda_4 v_\sigma^2 & \lambda_{14} v_\sigma v_\chi \\ \lambda_{14} v_\sigma v_\chi & -\frac{f v_\eta v_\rho}{\sqrt{2} v_\chi} + 2\lambda_1 v_\chi^2 \end{pmatrix}. \quad (72)$$

This matrix provides two physical states, $\mathcal{H}_{1(2)}, \mathcal{H}_{2(2)}$ which are related to the gauge eigenstates as below:

$$\begin{pmatrix} \mathcal{H}_{1(2)} \\ \mathcal{H}_{2(2)} \end{pmatrix} = \begin{pmatrix} \cos \beta_{1(2)} & \sin \beta_{1(2)} \\ -\sin \beta_{1(2)} & \cos \beta_{1(2)} \end{pmatrix} \begin{pmatrix} R_\sigma \\ R_\chi^3 \end{pmatrix}, \quad (73)$$

with the mixing angle defined as:

$$\tan 2\beta_{1(2)} = -\frac{4\lambda_{14} v_\sigma v_\chi^2}{\sqrt{2} f v_\eta v_\rho + 4\lambda_4 v_\sigma^2 v_\chi - 4\lambda_1 v_\chi^3}. \quad (74)$$

The masses of these two fields are given as

$$m_{\mathcal{H}_{1,2(2)}}^2 = \lambda_4 v_\sigma^2 + \lambda_1 v_\chi^2 - \frac{f v_\eta v_\rho}{2\sqrt{2} v_\chi} \pm \sqrt{\left(\frac{f v_\eta v_\rho}{2\sqrt{2} v_\chi}\right)^2 + \frac{f v_\eta v_\rho}{\sqrt{2} v_\chi} (\lambda_4 v_\sigma^2 - \lambda_1 v_\chi^2) + (\lambda_4 v_\sigma^2 - \lambda_1 v_\chi^2)^2 + \lambda_{14}^2 v_\sigma^2 v_\chi^2}. \quad (75)$$

In the basis $(R_\phi, R_\rho, R_\eta^1)$, the mass squared matrix is:

$$M_{even_{2b(2)}}^2 = \begin{pmatrix} 2\lambda_{35} v_\phi^2 & \lambda_{38} v_\rho v_\phi & \lambda_{37} v_\eta v_\phi \\ \lambda_{38} v_\rho v_\phi & -\frac{f v_\eta v_\chi}{\sqrt{2} v_\rho} + 2\lambda_3 v_\rho^2 & \lambda_{10} v_\eta v_\rho - \frac{f v_\chi}{\sqrt{2}} \\ \lambda_{37} v_\eta v_\phi & \lambda_{10} v_\eta v_\rho - \frac{f v_\chi}{\sqrt{2}} & -\frac{f v_\rho v_\chi}{\sqrt{2} v_\eta} + 2\lambda_2 v_\eta^2 \end{pmatrix}. \quad (76)$$

The determinant of the matrix above being non-zero implies the existence of three physical states. In general, the physical states are related to the gauge eigenstates through a 3×3 unitary matrix :

$$\begin{pmatrix} \mathcal{H}_{3(2)} \\ h_{(2)} \\ \mathcal{H}_{4(2)} \end{pmatrix} \simeq \begin{pmatrix} \cos \beta_{3(2)} & \sin \beta_{2(2)} \sin \beta_{3(2)} & -\cos \beta_{2(2)} \sin \beta_{3(2)} \\ -\sin \beta_{3(2)} & \sin \beta_{2(2)} \cos \beta_{3(2)} & -\cos \beta_{2(2)} \cos \beta_{3(2)} \\ 0 & \cos \beta_{2(2)} & \sin \beta_{2(2)} \end{pmatrix} \begin{pmatrix} R_\phi \\ R_\rho \\ R_\eta^1 \end{pmatrix}. \quad (77)$$

Assuming, $v_\phi \gg v_\rho, v_\eta$, we obtain the approximate values of the masses and the mixing angles in Appendix.C. We have identified two Higgs particles with masses at the EW scale. One of these two particles is identified as the SM Higgs-like boson, while the other may correspond to the light Higgs boson reported by the CMS collaboration [51].

IV. LEPTOGENESIS

Due to the presence of the three pairs of pseudo-Dirac heavy neutrinos, the model can explain the observed baryon asymmetry of the universe via resonant leptogenesis [22, 23, 25–27]. We focus on the one-loop model, as the analysis for the two-loop case will be very similar. The lightest pair of the heavy pseudo-Dirac neutrinos, ν_{R1}^\pm , with masses $M_{11}^\pm = (M \pm \mu)_{11}$, decay to produce a lepton asymmetry that can be enhanced by the small mass splitting between ν_{R1}^+ and ν_{R1}^- .

The CP asymmetry thus generated is given as [23],

$$\epsilon_\pm \simeq \frac{\text{Im} \left[\left((x_\rho^{(L)+})^\dagger x_\rho^{(L)-} \right)^2 \right]_{11}}{8\pi A_\pm} \frac{r}{r^2 + \frac{\Gamma_\pm^2}{M_1^{\mp 2}}} \quad (78)$$

where $x_\rho^{(L)\pm} = \frac{x_\rho^{(L)}}{\sqrt{2}}(1 \pm \frac{1}{4}M^{-1}\mu)$, $r = \frac{M_1^{+2} - M_1^{-2}}{M_1^+ M_1^-}$, $A_\pm = x_\rho^{(L)\dagger} x_\rho^{(L)}_\pm$ and $\Gamma_\pm = \frac{A_\pm M_{1\pm}}{8\pi}$.

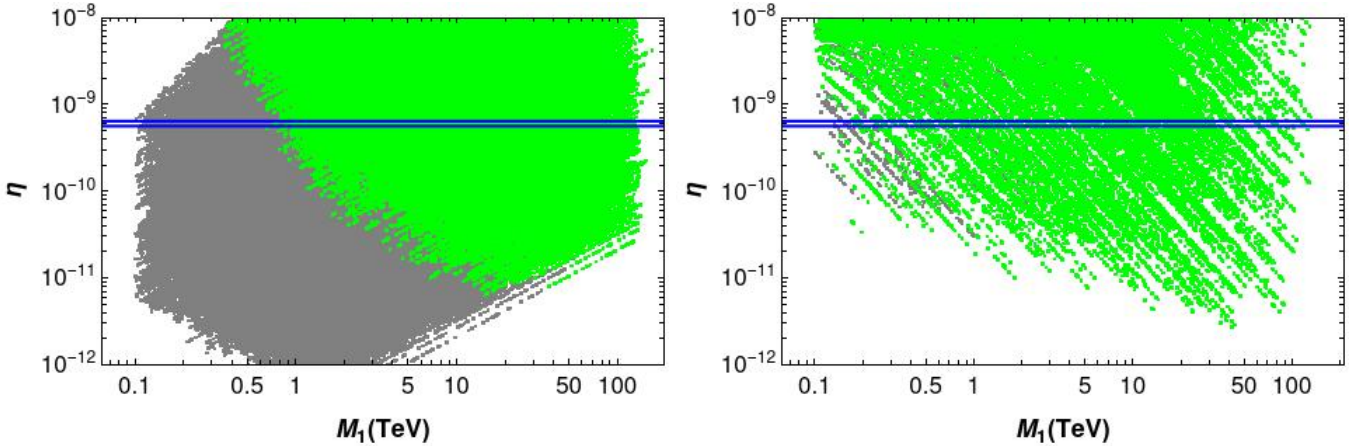


Figure 3: Baryon asymmetry parameter as a function of the mass of the lightest heavy neutrino. The figure in the left panel is for the parameter space with a weak washout, whereas the one in the right panel is for a strong washout. The horizontal blue lines correspond to the 3σ range of the observed baryon asymmetry of the universe. The gray points represent the correct active light neutrino masses, whereas the green points satisfy the bounds on the non-unitarity of the PMNS matrix.

Depending on the values of the couplings, leptogenesis can occur in either the strong washout regime or the weak washout regime. Assuming that the washout factor mainly depends on the inverse decay of the Higgs and charged lepton into the pseudo-Dirac neutrinos, the effective washout parameter is defined as,

$$K_N^{eff} \simeq \frac{\Gamma_+ + \Gamma_-}{H} \left(\frac{M_{1+} - M_{1-}}{\Gamma_\pm} \right)^2, \quad (79)$$

with $H = \sqrt{\frac{4\pi^3 g_*}{45}} \frac{T^2}{M_{Pl}}$ is the Hubble parameter. The expressions for the baryon asymmetry parameter in the weak

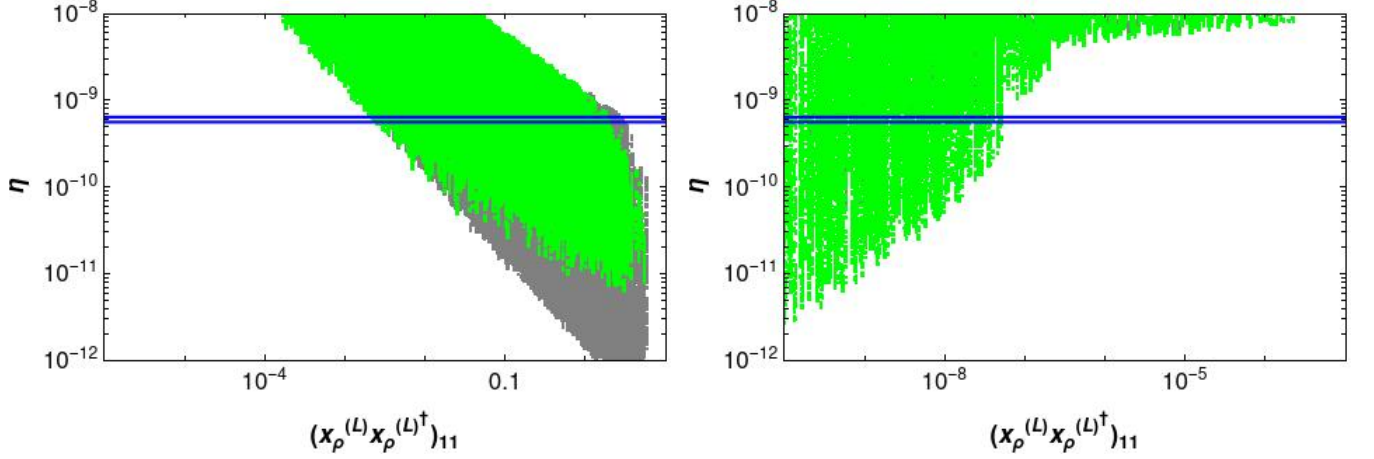


Figure 4: Baryon asymmetry as a function of $((x_\rho^{(L)})^\dagger x_\rho^{(L)})_{11}$. The figure in the left panel is for the parameter space with a weak washout whereas the one in the right panel is for a strong washout. The horizontal blue lines correspond to the 3σ range of the observed baryon asymmetry of the universe. The color codes are the same as in Fig. 3.

and strong washout regimes are approximately given as[52]:

$$\eta_B = \frac{\epsilon_\pm}{g_*} \quad \text{for } K_N^{eff} \ll 1, \quad (80)$$

$$\eta_B = \frac{0.3\epsilon_\pm}{g_* K_N^{eff} (\ln K_N^{eff})^{0.6}} \quad \text{for } K_N^{eff} \gg 1. \quad (81)$$

We emphasize that the model parameters influencing the baryon asymmetry, as defined above, also play a critical role in several other phenomena. These include the generation of light active neutrino masses, the non-unitarity of the neutrino mass mixing matrix, and processes involving lepton flavor violation. Fig. (3) displays the correlation of baryon asymmetry against the mass of the lightest heavy neutrino. The left panel represents the parameter space with a weak washout, while the right panel depicts a strong washout. The horizontal blue lines represent the 3σ range of the observed baryon asymmetry of the universe [4]. The gray points satisfy the bounds on active light neutrino masses and mixings as indicated by the oscillation experiments, whereas the green points satisfy the bounds on the non-unitarity of the PMNS matrix [53]. Fig. (4) depicts the correlation between baryon asymmetry and $((x_\rho^{(L)})^\dagger x_\rho^{(L)})_{11}$. Here also, the left panel represents the parameter space with a weak washout, while the right panel illustrates a strong washout. All the color codes are the same as in Fig. 3. From these figures, we can see that the parameter space that successfully explains the observed matter-antimatter asymmetry in the weak washout regime corresponds to larger values of the Yukawa couplings whereas the parameter space with strong washout corresponds to very small Yukawa couplings. Because of this, the weak washout case does not get constrained by the bounds from the non-unitarity of the PMNS matrix as the unitarity violation is very small in this case. Further, in the weak washout case, the correct baryon asymmetry is satisfied for the lightest heavy neutrino mass $M_1 \gtrsim 1$ TeV, whereas in the strong washout regime, this is satisfied even for M_1 as light as a few 100 GeV.

Fig. (5) illustrates the correlations between the mass of the lightest heavy neutrino and $((x_\rho^{(L)})^\dagger x_\rho^{(L)})_{11}$ for the parameter space that reproduces the correct value of the observed baryon asymmetry. The figures in the left and right panels correspond to the parameter spaces with weak washout and strong washout, respectively. The color scales represent the values of $BR(\mu \rightarrow e\gamma)$ for the corresponding points. Fig. (6) illustrates the correlation of the baryon asymmetry parameter with $BR(\mu \rightarrow e\gamma)$. The horizontal blue lines represent the 3σ experimentally allowed range of the observed baryon asymmetry of the universe, while the vertical red line corresponds to the MEG bound on $BR(\mu \rightarrow e\gamma)$. Similarly, the color codes are consistent with those ones used in Figs. 3 and 4. Once again, we can see that because of the small Yukawa couplings, the parameter space associated with the strong washout region predicts really small values for the branching ratio of the $\mu \rightarrow e\gamma$ decay, falling below the MEG limit. On the other hand, the weak washout case can give rise to larger values of $Br(\mu \rightarrow e\gamma)$ that could be observed in the future lepton flavor violating experiments.

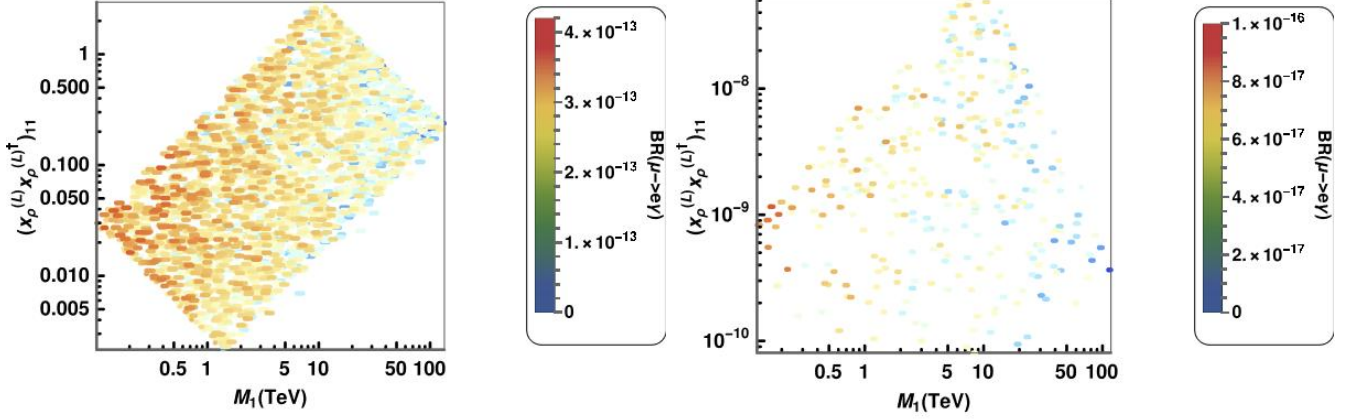


Figure 5: Correlations of the mass of the lightest heavy neutrino against $((x_\rho^{(L)})^\dagger x_\rho^{(L)})_{11}$ for the parameter space that reproduces the correct value of the observed baryon asymmetry. The figure in the left panel is for the parameter space with a weak washout whereas the one in the right panel is for a strong washout. The color scales show the values of $BR(\mu \rightarrow e\gamma)$ for the corresponding points.

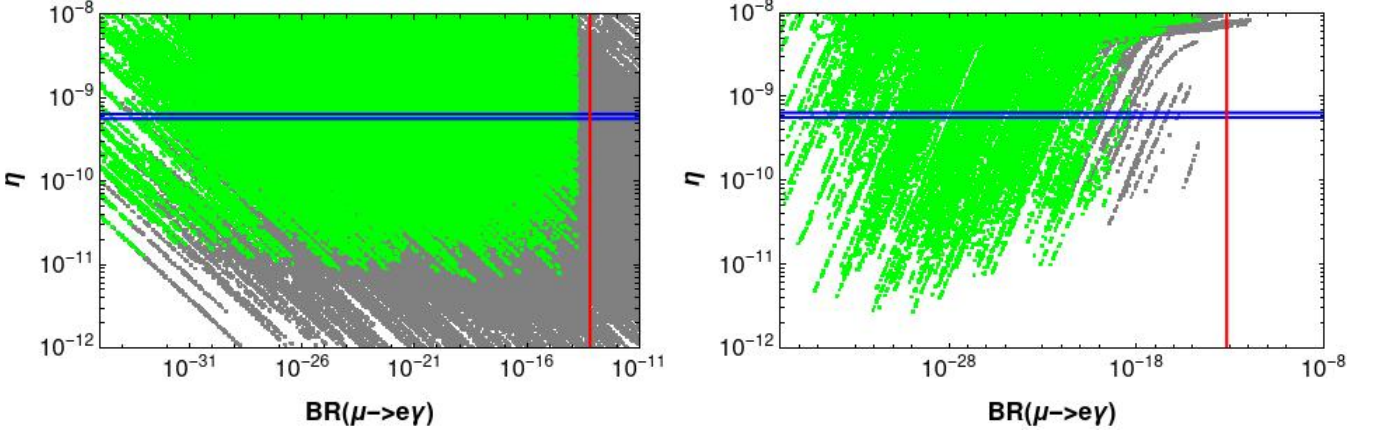


Figure 6: Correlation of the baryon asymmetry parameter against $BR(\mu \rightarrow e\gamma)$ for the scenarios of weak (left-panel) and strong (right-panel) washout. The horizontal blue lines correspond to the 3σ range of the observed baryon asymmetry of the universe whereas the vertical red line corresponds to the MEG bound on $BR(\mu \rightarrow e\gamma)$. The color codes are the same as in Fig. 3.

V. MUON AND ELECTRON ANOMALOUS MAGNETIC MOMENTS

In this section we discuss the implications of our models for the muon and electron anomalous magnetic moments. Given that the charged lepton sector is practically the same in both models (their differences are mainly in the scalar and neutrino sectors), the expressions for the muon and electron anomalous magnetic moments in the two models take the same form and are given by:

$$\begin{aligned} \Delta a_\mu \simeq & \sum_{k=1}^3 \sum_{j=1}^2 \frac{\text{Re}(\kappa_{2k} \gamma_{k2}^*) m_\mu^2}{8\pi^2} (R_{H(1)})_{1j} (R_{H(1)})_{2j} I_S^{(\mu)}(m_{E_k}, m_{\mathcal{H}_j}) \\ & + \sum_{k=1}^3 \frac{\text{Re}(\kappa_{2k} \gamma_{k2}^*) m_\mu^2}{8\pi^2} (R_{H(1)})_{13} (R_{H(1)})_{23} I_S^{(\mu)}(m_{E_k}, m_h), \end{aligned} \quad (82)$$

$$\Delta a_e \simeq \sum_{k=1}^3 \sum_{j=1}^2 \frac{\text{Re}(\kappa_{1k} \gamma_{k1}^*) m_\mu^2}{8\pi^2} (R_{H(1)})_{1j} (R_{H(1)})_{2j} I_S^{(e)}(m_{E_k}, m_{\mathcal{H}_j}) \\ + \sum_{k=1}^3 \frac{\text{Re}(\kappa_{1k} \gamma_{k1}^*) m_\mu^2}{8\pi^2} (R_{H(1)})_{13} (R_{H(1)})_{23} I_S^{(e)}(m_{E_k}, m_h), \quad (83)$$

where, the loop function $I_{S(P)}^{(e,\mu)}(m_E, m)$ has the form [54–58]:

$$I_{S(P)}^{(e,\mu)}(m_E, m_S) = \int_0^1 \frac{x^2 \left(1 - x \pm \frac{m_E}{m_{e,\mu}}\right)}{m_{e,\mu}^2 x^2 + (m_E^2 - m_{e,\mu}^2)x + m_{S,P}^2(1-x)} dx. \quad (84)$$

In Eqs.(82) and (83), m_{E_k} correspond to the masses of exotic charged leptons E_k and $m_{S,P}$ are the masses of scalar or pseudoscalar fields. The matrix $R_{H(1)}$ corresponds to the rotational matrix that diagonalizes the CP even scalar mass matrix. In general, it is a 3×3 orthogonal matrix.

Besides, the dimensionless parameters β_{1k} , β_{2k} , γ_{j1} , and γ_{j2} are given by:

$$\kappa_{1j} = \sum_{i=1}^3 y_{ij}^{(E)} (V_{iL}^\dagger)_{1i}, \quad \gamma_{j1} = \sum_{j=1}^3 y_{kj}^{(l)} (V_{lR})_{j1}, \quad (85)$$

$$\kappa_{2j} = \sum_{i=1}^3 y_{ij}^{(E)} (V_{iL}^\dagger)_{2i}, \quad \gamma_{j1} = \sum_{j=1}^3 y_{kj}^{(l)} (V_{lR})_{j2}, \quad (86)$$

where V_{iL} and V_{iR} are the rotational matrices that diagonalize \widetilde{M}_l according to the relation:

$$V_{iL}^\dagger \widetilde{M}_l V_{iR} = \text{diag}(m_e, m_\mu, m_\tau). \quad (87)$$

The experimentally measured values of the anomalous magnetic moments of the muon and electron are given as [59, 60]:

$$(\Delta a_\mu)_{\text{exp}} = (2.49 \pm 0.48) \times 10^{-9} \\ (\Delta a_e)_{\text{exp}} = (4.8 \pm 3.0) \times 10^{-13}. \quad (88)$$

Since the value of the electron anomalous magnetic moment (Δa_e) is much smaller than that of the muon anomalous magnetic moment (Δa_μ), one can focus solely on Δa_e to establish reasonable correlations. In Fig.(7), we plot the correlation of the electron anomalous magnetic moment Δa_e against the mass of the charged exotic lepton E_1 . The predictions for the muon anomalous magnetic moment are shown by the color scale. It can be seen from this figure that when the mass of E_1 varies from 100 GeV to 250 GeV, the prediction for Δa_μ takes values up to a maximum of 3.5×10^{-9} whereas the predictions for Δa_e varies from 8×10^{-13} to 0.5×10^{-13} . Clearly, the value of the anomalous magnetic moment decreases with the increase in the mass of the charged exotic lepton. As seen from Fig. 7, our proposed models are capable of successfully accommodating the experimental values of the muon and electron anomalous magnetic moments.

VI. CONCLUSIONS

We have developed two models aimed at explaining the tiny masses of active light neutrinos. Both models employ the inverse seesaw mechanism to generate small neutrino masses and the leptonic mixing angles. In the first model, this is realized at the one-loop level, while in the second model, the inverse seesaw is realized at the two-loop level. Both models are extensions of the conventional 3-3-1 models, where the gauge symmetry $SU(3)_C \times SU(3)_L \times U(1)_X$ is augmented by the inclusion of the generalized global lepton number symmetry $U(1)_{L_g}$. The spontaneous breaking of $U(1)_{L_g}$ to a preserved Z_2 symmetry ensures the radiative nature of the inverse seesaw mechanisms. Accomplishing this necessitates an extension of the fermion and scalar spectrum beyond the simplest versions of 3-3-1 models. Furthermore, in these models, the masses of the charged leptons in the SM arise from a tree-level seesaw mechanism. We have thoroughly examined the mass spectra of scalar particles in the two models.

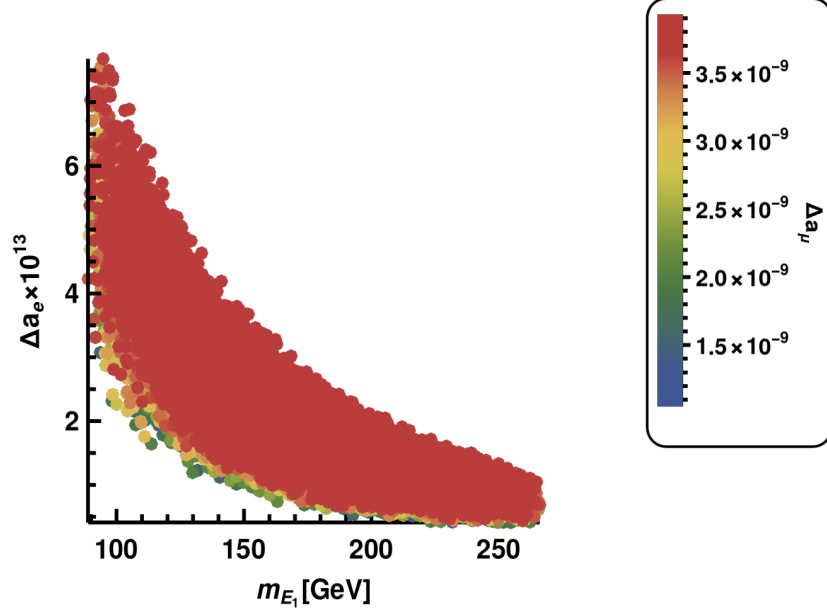


Figure 7: Corellation between Δa_e and mass of charged lepton E_1 .

Assuming that two of the scalars acquire VEVs of the order of EW scale, we note that there can be two CP-even scalar particles with masses in the range $100 - 200$ GeV. One of them corresponds to the SM Higgs boson of mass 125 GeV whereas the other could potentially be the Higgs boson with a mass of 150 GeV, as announced by the CMS collaboration.

We have also studied the parameter space for successful resonant leptogenesis focusing on the combined constraints from the light neutrino masses and mixings, non-unitarity of the PMNS matrix, and charged lepton flavor violation. We found that the model can simultaneously explain the observed baryon asymmetry and satisfy the experimental constraints, for both strong as well as weak washout regimes. We have also studied the contributions of the exotic vector-like charged leptons to the electron and muon anomalous magnetic moments and found that the model satisfies the experimental observations for charged exotic leptons in the mass range $100 - 250$ GeV.

Acknowledgments

RIP Iván, it was an honor to collaborate with you. The work of C.B. was supported by ANID-Chile FONDECYT Regular No. 1241855. AECH was funded by Chilean grants ANID-Chile FONDECYT 1210378, ANID PIA/APOYO AFB230003, ANID- Programa Milenio - code ICN2019_044 and ANID-Chile FONDECYT Regular No. 1241855. V.K.N. is supported by ANID-Chile Fondecyt Postdoctoral grant 3220005. DTH acknowledges the financial support of the International Centre of Physics, Institute of Physics, VAST under Grant No.ICP-2024.02.

Appendix A: Radiative generation of the μ -term

μ -term at one-loop

Here we give a list of conditions satisfied by Model-1 to have a μ matrix generated at the one-loop level. Fields and charge assignments in Tables I, II and III allow the existence of following operators:

$$\bar{N}_{iR} \Psi_{nR}^C \varphi, \quad (m_\Psi)_{nk} \bar{\Psi}_{nR} \Psi_{kR}^C, \quad \varphi^2 \sigma, \quad (\text{with } i = 1, 2, 3, \text{ and } n, k = 1, 2) \quad (\text{A1})$$

and forbid a tree-level operator:

$$(m_N)_{ij} \bar{N}_{iR} N_{jR}^C, \quad (\text{with } i, j = 1, 2, 3), \quad (\text{A2})$$

where N_{iR} ($i = 1, 2, 3$) and Ψ_{nR} ($n = 1, 2$) are right-handed Majorana neutrinos, whereas φ and σ are electrically neutral-gauge singlet scalars.

The submatrices m and M are generated via the following operators:

$$\varepsilon_{abc} \bar{L}_{iL}^a (L_{jL}^C)^b (\rho^*)^c, \quad \bar{L}_{iL} \chi N_{jR}, \quad (\text{A3})$$

where L_{iL} ($i = 1, 2, 3$) and ρ are $SU(3)_L$ leptonic and scalar triplets, respectively.

Furthermore, the SM-charged lepton masses are generated from a tree-level seesaw mechanism with the charged lepton mass matrix in the basis $(\bar{l}_{iL}, \bar{E}_{iL}) - (\bar{l}_{iR}, \bar{E}_{iR})$ taking the following structure:

$$M_l = \begin{pmatrix} 0_{3 \times 3} & A \\ B^T & M_E \end{pmatrix}, \quad (\text{A4})$$

where $i = 1, 2, 3$, E_i are charged exotic vector-like fermions and A , B and M_E are 3×3 matrices. Thus, the successful implementation of the tree-level seesaw mechanism to generate the SM-charged lepton masses requires that the operators:

$$\bar{l}_{iL} \rho E_{jR}, \quad \bar{E}_{iL} \xi l_{jR}, \quad (M_E)_{ij} \bar{E}_{iL} E_{jR}, \quad (\text{A5})$$

are forbidden whereas the operator:

$$\bar{l}_{iL} \rho l_{jR}, \quad (\text{A6})$$

is to be forbidden. This is guaranteed by discrete Z_2 symmetry.

Note that in addition to generating the SM-charged lepton masses via a seesaw-like mechanism, the inclusion of the exotic fermions E_i also helps in successfully accommodating the experimental values of the muon and electron anomalous magnetic moments.

μ -term at two-loops

Now we proceed to discuss the considerations taken to generate the submatrix μ at the two-loop level in what we call Model-2. The particle content and charge assignments given in Tables IV, V, and VI, guarantee the existence of the following operators:

$$\bar{L}_{iL} \chi N_{jR}, \quad \bar{\Psi}_{kR}^C \xi^+ l_{kR}, \quad \bar{N}_{nR}^C \varphi \Psi_{kR}, \quad (m_\Psi)_{nk} \Psi_{nR} \bar{\Psi}_{kR}^C, \quad (\text{A7})$$

$$\xi^- \zeta^+ \sigma^2, \quad \chi^\dagger \rho \zeta^- \varphi^*, \quad (\text{A8})$$

and forbid operators of the form:

$$(m_N)_{ij} \bar{N}_{iR} N_{jR}^C, \quad \varphi^2 (\sigma^\dagger), \quad \varphi^2 \sigma, \quad \varphi^2 (\sigma^\dagger)^2, \quad \varphi^2 \sigma^2, \quad i, j = 1, 2, 3, \quad (\text{A9})$$

where σ and φ are electrically neutral scalar singlets as before. ζ^\pm and ξ^\pm are electrically charged scalars whereas η , χ and ρ are $SU(3)_L$ scalar triplets. Once again, the generation of the submatrix μ at two-loop level requires the inclusion of a spontaneously broken $U(1)_{L_g}$ symmetry that gets broken spontaneously to a remnant preserved \tilde{Z}_2 symmetry.

Under this \tilde{Z}_2 symmetry, the scalar field φ has a non-zero charge and thus it does not acquire a vacuum expectation value (VEV). The \tilde{Z}_2 symmetry is crucial to forbid mass terms of the form $(m_{N\Psi})_{nk} \bar{N}_{nR}^C \Psi_{kR}$ that would result in a tree-level generation of the Majorana submatrix μ . Furthermore, in this realization of the two-loop level inverse seesaw mechanism, the SM-charged lepton masses are generated via seesaw mechanism mediated by the following operators:

$$\bar{l}_{iL} \rho E_{jR}, \quad \bar{E}_{iL} \phi l_{jR}, \quad \bar{E}_{iL} \sigma E_{jR}, \quad (\text{A10})$$

Similar to the situation in Model-1, the $U(1)_{L_g}$ symmetry forbids the operator:

$$\bar{l}_{iL}\rho l_{jR}, \quad (\text{A11})$$

leading to a successful two-loop generation mechanism.

Appendix B: Diagonalizing the mass matrix of the CP-even sectors in the model 1

In the basis $(R_\xi, R_\rho, R_\eta^1)$, the mass squared matrix is:

$$\begin{aligned} M_{even2b(1)}^2 &= \begin{pmatrix} 2\lambda_6 v_\xi^2 - \frac{Bv_\eta v_\rho v_\chi}{2v_\xi} & \frac{Bv_\eta v_\chi}{2} + \lambda_{20} v_\xi v_\rho & \frac{Bv_\rho v_\chi}{2} + \lambda_{21} v_\eta v_\xi \\ 2\lambda_3 v_\rho^2 - \frac{Bv_\eta v_\xi v_\chi}{2v_\rho} & \frac{Bv_\xi v_\chi}{2} + \lambda_9 v_\eta v_\rho & 2\lambda_2 v_\eta^2 - \frac{Bv_\xi v_\rho v_\chi}{2v_\eta} \end{pmatrix} \\ &= 2v_\chi \begin{pmatrix} \frac{\lambda_6 v_\xi^2}{v_\chi} - \frac{Bv_\eta v_\rho}{4v_\xi} & \frac{Bv_\eta}{4} + \frac{\lambda_{20} v_\xi v_\rho}{2v_\chi} & \frac{Bv_\rho}{4} + \frac{\lambda_{21} v_\eta v_\xi}{2v_\chi} \\ \frac{\lambda_3 v_\rho^2}{v_\chi} - \frac{Bv_\eta v_\xi}{4v_\rho} & \frac{Bv_\xi}{4} + \frac{\lambda_9 v_\eta v_\rho}{2v_\chi} & \frac{\lambda_2 v_\eta^2}{v_\chi} - \frac{Bv_\xi v_\rho}{4v_\eta} \end{pmatrix}. \end{aligned} \quad (\text{B1})$$

We take the limit $v_\sigma, v_\chi \gg v_\xi, v_\eta, v_\rho$, so that the terms that are inversely proportional to v_χ in the matrix $M_{even2b(1)}^2$ can be ignored. Then, the approximate form of the matrix $M_{even2b(1)}^2$ becomes:

$$M_{even2B(1)}^2 = \frac{Bv_\chi}{2} \begin{pmatrix} -\frac{v_\eta v_\rho}{v_\xi} & v_\eta & v_\rho \\ -\frac{v_\eta v_\xi}{v_\rho} & v_\xi & -\frac{v_\xi v_\rho}{v_\eta} \end{pmatrix} = \frac{-Bv_\chi}{2} M_{e2(1)}. \quad (\text{B2})$$

The 2×2 block on the right bottom of $M_{even2B(1)}^2$ may be rewritten as:

$$M_{e2(1)}^2 = \frac{-Bv_\chi v_\xi}{2} \begin{pmatrix} \frac{v_\eta}{v_\rho} & 1 \\ 1 & \frac{v_\rho}{v_\eta} \end{pmatrix}. \quad (\text{B3})$$

After diagonalizing, the matrix $M_{e2(1)}^2$ has form:

$$M_{e2(1)}^{2diag} = \frac{-Bv_\chi v_\xi}{2} \begin{pmatrix} 0 & 0 \\ 0 & \frac{v_\rho}{v_\eta} + \frac{v_\eta}{v_\rho} \end{pmatrix}. \quad (\text{B4})$$

Thus, we get a massive state $h_{(1)} = \cos \beta_{2(1)} R_\rho + \sin \beta_{2(1)} R_\eta^1$. This could be the SM-like Higgs boson (SMLHB) whose mass is:

$$m_{h(1)}^2 = \frac{-Bv_\chi v_\xi}{2} \left(\frac{v_\rho}{v_\eta} + \frac{v_\eta}{v_\rho} \right) = \frac{-Bv_\chi v_\xi v^2}{2v_\rho v_\eta}, \quad (\text{B5})$$

where $v^2 = v_\rho^2 + v_\eta^2 = 246^2$ GeV and the parameter B should be negative with the absolute value of Bv_χ being in the EW scale as v_ξ, v_ρ, v_η . The matrix $M_{e2(1)}^2$ in Eq. (B4) is diagonalized by a 2×2 orthogonal matrix parametrized by the mixing angle $\beta_{2(1)}$ which is given by:

$$\tan \beta_{2(1)} = \frac{v_\rho}{v_\eta} = -\cot \alpha_{1(1)}. \quad (\text{B6})$$

Hence, the matrix that is used to diagonalize the matrix $M_{e2(1)}^2$ is:

$$U_{\beta_{2(1)}} = \begin{pmatrix} \sin \beta_{2(1)} & -\cos \beta_{2(1)} \\ \cos \beta_{2(1)} & \sin \beta_{2(1)} \end{pmatrix}. \quad (\text{B7})$$

Coming to the diagonalization of the original 3×3 mass squared matrix, the above 2×2 can be represented as a 3×3 rotational matrix with the following form:

$$U_{\beta_{2s(1)}} = \begin{pmatrix} 1 & 0 & 0 \\ 0 & \sin \beta_{2(1)} & -\cos \beta_{2(1)} \\ 0 & \cos \beta_{2(1)} & \sin \beta_{2(1)} \end{pmatrix}. \quad (\text{B8})$$

This $U_{\beta_{2s(1)}}$ matrix changes the matrix $M_{even2B(1)}^2$ defined in B3 to another form:

$$M_{e2s(1)} = -\frac{Bv_\chi}{2} \begin{pmatrix} -\frac{v_\eta v_\rho}{v_\xi} & \frac{2v_\rho v_\eta}{v} & \frac{v_\rho^2 - v_\eta^2}{v} \\ \frac{2v_\rho v_\eta}{v} & 0 & 0 \\ \frac{v_\rho^2 - v_\eta^2}{v} & 0 & -\frac{v_\xi(v_\eta^2 + v_\rho^2)}{v_\eta v_\rho} \end{pmatrix}. \quad (\text{B9})$$

If $v_\eta \approx v_\rho$, the third element of the first row (as well as the first element of the third row) in the matrix $M_{e2s(1)}$ can be ignored. The matrix $M_{e2s(1)}$ is then rewritten as:

$$M_{e2r(1)} = -\frac{Bv_\chi}{2} \begin{pmatrix} -\frac{v_\eta v_\rho}{v_\xi} & \frac{2v_\rho v_\eta}{v} & 0 \\ \frac{2v_\rho v_\eta}{v} & 0 & 0 \\ 0 & 0 & -\frac{v_\xi v^2}{v_\eta v_\rho} \end{pmatrix}. \quad (\text{B10})$$

The 2×2 block on the left top of $M_{e2r(1)}$ is rewritten as:

$$M_{e2r(1)} = -\frac{Bv_\chi}{2} \begin{pmatrix} -\frac{v_\eta v_\rho}{v_\xi} & \frac{2v_\rho v_\eta}{v} \\ \frac{2v_\rho v_\eta}{v} & 0 \end{pmatrix}. \quad (\text{B11})$$

This $M_{e2r(1)}$ matrix is diagonalized by the matrix:

$$U_{\beta_{3(1)}} = \begin{pmatrix} \cos \beta_{3(1)} & \sin \beta_{3(1)} \\ -\sin \beta_{3(1)} & \cos \beta_{3(1)} \end{pmatrix}. \quad (\text{B12})$$

Then, we receive a 3×3 rotational matrix with the form below:

$$U_{\beta_{3s(1)}} = \begin{pmatrix} \cos \beta_{3(1)} & \sin \beta_{3(1)} & 0 \\ \sin \beta_{3(1)} & \cos \beta_{3(1)} & 0 \\ 0 & 0 & 1 \end{pmatrix}. \quad (\text{B13})$$

with the mixing angle $\beta_{3(1)}$ defined as:

$$\tan \beta_{3(1)} = \frac{\sqrt{v^2 + 8v_\xi^2} - v\sqrt{v^2 + 16v_\xi^2}}{2\sqrt{2}v_\xi}. \quad (\text{B14})$$

Then, the physical states are:

$$\begin{aligned} \mathcal{H}_{3(1)} &= R_\xi \cos \beta_{3(1)} + R_\rho \sin \beta_{3(1)}, \\ \mathcal{H}_{4(1)} &= -R_\xi \sin \beta_{3(1)} + R_\rho \cos \beta_{3(1)}. \end{aligned} \quad (\text{B15})$$

The masses of these two physical states are:

$$m_{\mathcal{H}_{3,4(1)}}^2 = -\frac{Bv_\chi v_\rho v_\eta}{4vv_\xi} \left(\sqrt{v^2 + 16v_\xi^2} \pm v \right). \quad (\text{B16})$$

Since $B \sim \frac{1}{v_\chi}$, $\mathcal{H}_{4(1)}$ acquires a mass at the same scale as SMLHB. The mass of $\mathcal{H}_{3(1)}$ could be in the TeV or subTeV scale. Finally, the matrix that diagonalizes the full 3×3 matrix $M_{even2b(1)}^2$ is:

$$\begin{aligned} U_{even2b(1)} &= U_{\beta_{3s(1)}} U_{\beta_{2s(1)}} \\ &= \begin{pmatrix} \cos \beta_{3(1)} & \sin \beta_{2(1)} \sin \beta_{3(1)} & -\cos \beta_{2(1)} \sin \beta_{3(1)} \\ -\sin \beta_{3(1)} & \sin \beta_{2(1)} \cos \beta_{3(1)} & -\cos \beta_{2(1)} \cos \beta_{3(1)} \\ 0 & \cos \beta_{2(1)} & \sin \beta_{2(1)} \end{pmatrix}. \end{aligned} \quad (\text{B17})$$

Appendix C: Diagonalizing the mass mixing matrix of the CP-even sectors in the model 2

In the basis $(R_\phi, R_\rho, R_\eta^1)$, the mass squared matrix has the form:

$$M_{even2b(2)}^2 = \begin{pmatrix} 2\lambda_{35}v_\phi^2 & \lambda_{38}v_\rho v_\phi & \lambda_{37}v_\eta v_\phi \\ \lambda_{38}v_\rho v_\phi & -\frac{fv_\eta v_\chi}{\sqrt{2}v_\rho} + 2\lambda_3v_\rho^2 & \lambda_{10}v_\eta v_\rho - \frac{fv_\chi}{\sqrt{2}} \\ \lambda_{37}v_\eta v_\phi & \lambda_{10}v_\eta v_\rho - \frac{fv_\chi}{\sqrt{2}} & -\frac{fv_\rho v_\chi}{\sqrt{2}v_\eta} + 2\lambda_2v_\eta^2 \end{pmatrix}. \quad (C1)$$

The 2×2 block on the right bottom of the matrix $M_{even2b(2)}^2$ in Eq. (C1) can be rewritten as:

$$M_{even2bs(2)}^2 = \begin{pmatrix} 2\lambda_3v_\rho^2 - \frac{fv_\eta v_\chi}{\sqrt{2}v_\rho} & \frac{fv_\chi}{\sqrt{2}} + \lambda_{10}v_\eta v_\rho \\ \frac{fv_\chi}{\sqrt{2}} + \lambda_{10}v_\eta v_\rho & 2\lambda_2v_\eta^2 - \frac{fv_\rho v_\chi}{\sqrt{2}v_\eta} \end{pmatrix} = -\frac{fv_\chi}{\sqrt{2}} \begin{pmatrix} \frac{v_\eta}{v_\rho} & 1 \\ 1 & \frac{v_\rho}{v_\eta} \end{pmatrix}. \quad (C2)$$

Then we get a massive state $h_{(2)} = \cos \beta_{2(2)} R_\rho + \sin \beta_{2(2)} R_\eta^1$. This might be the SM-like Higgs boson (SMLHB) whose mass is:

$$m_{h_{(2)}}^2 = \frac{-fv_\chi v^2}{\sqrt{2}v_\rho v_\eta}, \quad (C3)$$

where $v^2 = v_\rho^2 + v_\eta^2 = (246 \text{ GeV})^2$ and the parameter f should be negative with its absolute value is $\sim \frac{1}{v_\chi}$. The mixing angle $\beta_{2(2)}$ is defined by the equation $\tan \beta_{2(2)} = \tan \beta_{2(1)} = -\cot \alpha_{1(1)}$.

Correspondingly, we get a 3×3 matrix as below:

$$U_{\beta_{2(2)}} = \begin{pmatrix} 1 & 0 & 0 \\ 0 & \cos \beta_{2(2)} & \sin \beta_{2(2)} \\ 0 & \sin \beta_{2(2)} & \cos \beta_{2(2)} \end{pmatrix}. \quad (C4)$$

The matrix $U_{\beta_{2(2)}}$ transforms the matrix $M_{even2b(2)}^2$ into another form:

$$M_{even2br(2)}^2 = \begin{pmatrix} 2\lambda_{35}v_\phi^2 & \frac{v_\phi(\lambda_{37}v_\eta^2 + \lambda_{38}v_\rho^2)}{v_\eta \sqrt{\frac{v_\rho^2}{v_\eta^2} + 1}} & \frac{(\lambda_{37} - \lambda_{38})v_\eta v_\phi}{\sqrt{\frac{v_\rho^2}{v_\eta^2} + 1}} \\ \frac{v_\phi(\lambda_{37}v_\eta^2 + \lambda_{38}v_\rho^2)}{v_\eta \sqrt{\frac{v_\rho^2}{v_\eta^2} + 1}} & \frac{2(\lambda_2v_\eta^4 + \lambda_{10}v_\eta^2v_\rho^2 + \lambda_3v_\rho^4)}{v_\eta^2 + v_\rho^2} & \frac{2\lambda_2v_\eta^2 + \lambda_{10}(v_\rho - v_\eta)(v_\eta + v_\rho) - 2\lambda_3v_\rho^2}{\sqrt{\frac{v_\rho^2}{v_\eta^2} + 1} \sqrt{\frac{v_\rho^2}{v_\eta^2} + 1}} \\ \frac{(\lambda_{37} - \lambda_{38})v_\eta v_\phi}{\sqrt{\frac{v_\rho^2}{v_\eta^2} + 1}} & \frac{2\lambda_2v_\eta^2 + \lambda_{10}(v_\rho - v_\eta)(v_\eta + v_\rho) - 2\lambda_3v_\rho^2}{\sqrt{\frac{v_\rho^2}{v_\eta^2} + 1} \sqrt{\frac{v_\rho^2}{v_\eta^2} + 1}} & \frac{2(\lambda_2 + \lambda_3 - \lambda_{10})v_\eta^2v_\rho^2}{v_\eta^2 + v_\rho^2} - \frac{fv_\chi}{(v_\eta^2 + v_\rho^2)} \sqrt{2}v_\eta v_\rho \end{pmatrix}. \quad (C5)$$

With the assumption that $\lambda_{37} \approx \lambda_{38}$, $\lambda_2 \approx \lambda_3 \approx \lambda_{10}$ and $v_\rho \approx v_\eta$, the matrix $M_{even2br(2)}^2$ might be rewritten as below:

$$M_{even2bt(2)}^2 = \begin{pmatrix} 2\lambda_{35}v_\phi^2 & \lambda_{37}v_\rho v_\phi & 0 \\ \lambda_{37}v_\rho v_\phi & \frac{3}{2}f^2\lambda_2v_\rho^2v_\chi^2 & 0 \\ 0 & 0 & \lambda_2v_\rho^2 - \sqrt{2}fv_\chi \end{pmatrix}. \quad (C6)$$

The 2×2 block on the left top of the matrix $M_{even2bt(2)}^2$ gives two massive bosons whose physical states are related to the gauge eigenstates as:

$$\begin{pmatrix} \mathcal{H}_{3(2)} \\ \mathcal{H}_{4(2)} \end{pmatrix} = \begin{pmatrix} \cos \beta_{3(2)} & \sin \beta_{3(2)} \\ -\sin \beta_{3(2)} & \cos \beta_{3(2)} \end{pmatrix} \begin{pmatrix} R_\phi \\ R_\rho \end{pmatrix}, \quad (C7)$$

where the mixing angle $\beta_{3(2)}$ is defined by:

$$\tan \beta_{3(2)} = \frac{2\lambda_{35}v_\phi^2 - 3\lambda_2v_\rho^2 - \sqrt{(3\lambda_2v_\rho^2 - 2\lambda_{35}v_\phi^2)^2 + 8\lambda_{37}^2v_\rho^2v_\phi^2}}{2\sqrt{2}\lambda_{37}v_\rho v_\phi}. \quad (C8)$$

The masses of these two scalars are:

$$m_{\mathcal{H}_{3,4(2)}}^2 = \frac{3\lambda_2 v_\rho^2}{2} + \lambda_{35} v_\phi^2 \pm \frac{1}{2} \sqrt{\left(3\lambda_2 v_\rho^2 - 2\lambda_{35} v_\phi^2\right)^2 + 8\lambda_{37}^2 v_\rho^2 v_\phi^2}. \quad (\text{C9})$$

Finally, the matrix which diagonalizes the matrix $M_{\text{even}2b(1)}^2$ is:

$$\begin{aligned} U_{\text{even}2b(2)} &= U_{\beta_{3s(1)}} U_{\beta_{2s(1)}} \\ &= \begin{pmatrix} \cos \beta_{3(2)} & \sin \beta_{2(2)} \sin \beta_{3(2)} & -\cos \beta_{2(2)} \sin \beta_{3(2)} \\ -\sin \beta_{3(2)} & \sin \beta_{2(2)} \cos \beta_{3(2)} & -\cos \beta_{2(2)} \cos \beta_{3(2)} \\ 0 & \cos \beta_{2(2)} & \sin \beta_{2(2)} \end{pmatrix}. \end{aligned} \quad (\text{C10})$$

-
- [1] A. B. McDonald, “Nobel Lecture: The Sudbury Neutrino Observatory: Observation of flavor change for solar neutrinos,” *Rev.Mod.Phys.* **88** (2016) 030502.
 - [2] T. Kajita, “Nobel Lecture: Discovery of atmospheric neutrino oscillations,” *Rev.Mod.Phys.* **88** (2016) 030501.
 - [3] P. de Salas *et al.*, “2020 global reassessment of the neutrino oscillation picture,” *JHEP* **02** (2021) 071, [arXiv:2006.11237 \[hep-ph\]](#).
 - [4] Planck Collaboration, N. Aghanim *et al.*, “Planck 2018 results. VI. Cosmological parameters,” *Astron. Astrophys.* **641** (2020) A6, [arXiv:1807.06209 \[astro-ph.CO\]](#). [Erratum: *Astron.Astrophys.* 652, C4 (2021)].
 - [5] C. A. de Sousa Pires and O. P. Ravinez, “Charge quantization in a chiral bilepton gauge model,” *Phys. Rev. D* **58** (1998) 035008, [arXiv:hep-ph/9803409](#).
 - [6] P. V. Dong and H. N. Long, “Electric charge quantization in SU(3)(C) x SU(3)(L) x U(1)(X) models,” *Int. J. Mod. Phys. A* **21** (2006) 6677–6692, [arXiv:hep-ph/0507155](#).
 - [7] J. C. Montero, V. Pleitez, and O. Ravinez, “Soft superweak CP violation in a 331 model,” *Phys. Rev. D* **60** (1999) 076003, [arXiv:hep-ph/9811280](#).
 - [8] J. C. Montero, C. C. Nishi, V. Pleitez, O. Ravinez, and M. C. Rodriguez, “Soft CP violation in K meson systems,” *Phys. Rev. D* **73** (2006) 016003, [arXiv:hep-ph/0511100](#).
 - [9] P. B. Pal, “The Strong CP question in SU(3)(C) x SU(3)(L) x U(1)(N) models,” *Phys. Rev. D* **52** (1995) 1659–1662, [arXiv:hep-ph/9411406](#).
 - [10] A. G. Dias, V. Pleitez, and M. D. Tonasse, “Naturally light invisible axion in models with large local discrete symmetries,” *Phys. Rev. D* **67** (2003) 095008, [arXiv:hep-ph/0211107](#).
 - [11] A. G. Dias and V. Pleitez, “Stabilizing the invisible axion in 3-3-1 models,” *Phys. Rev. D* **69** (2004) 077702, [arXiv:hep-ph/0308037](#).
 - [12] A. G. Dias, C. A. de S. Pires, and P. S. Rodrigues da Silva, “Discrete symmetries, invisible axion and lepton number symmetry in an economic 3 3 1 model,” *Phys. Rev. D* **68** (2003) 115009, [arXiv:hep-ph/0309058](#).
 - [13] J. K. Mizukoshi, C. A. de S. Pires, F. S. Queiroz, and P. S. Rodrigues da Silva, “WIMPs in a 3-3-1 model with heavy Sterile neutrinos,” *Phys. Rev. D* **83** (2011) 065024, [arXiv:1010.4097 \[hep-ph\]](#).
 - [14] A. G. Dias, C. A. de S. Pires, and P. S. Rodrigues da Silva, “The Left-Right SU(3)(L)xSU(3)(R)xU(1)(X) Model with Light, keV and Heavy Neutrinos,” *Phys. Rev. D* **82** (2010) 035013, [arXiv:1003.3260 \[hep-ph\]](#).
 - [15] J. D. Ruiz-Alvarez, C. A. de S. Pires, F. S. Queiroz, D. Restrepo, and P. S. Rodrigues da Silva, “On the Connection of Gamma-Rays, Dark Matter and Higgs Searches at LHC,” *Phys. Rev. D* **86** (2012) 075011, [arXiv:1206.5779 \[hep-ph\]](#).
 - [16] D. Cogollo, A. X. Gonzalez-Morales, F. S. Queiroz, and P. R. Teles, “Excluding the Light Dark Matter Window of a 331 Model Using LHC and Direct Dark Matter Detection Data,” *JCAP* **11** (2014) 002, [arXiv:1402.3271 \[hep-ph\]](#).
 - [17] P. S. Rodrigues da Silva, “A Brief Review on WIMPs in 331 Electroweak Gauge Models,” *Phys. Int.* **7** no. 1, (2016) 15–27, [arXiv:1412.8633 \[hep-ph\]](#).
 - [18] R. Mohapatra and J. Valle, “Neutrino Mass and Baryon Number Nonconservation in Superstring Models,” *Phys. Rev. D* **34** (1986) 1642.
 - [19] E. K. Akhmedov, M. Lindner, E. Schnapka, and J. W. F. Valle, “Left-right symmetry breaking in NJL approach,” *Phys. Lett. B* **368** (1996) 270–280, [arXiv:hep-ph/9507275](#).
 - [20] E. K. Akhmedov, M. Lindner, E. Schnapka, and J. W. F. Valle, “Dynamical left-right symmetry breaking,” *Phys. Rev. D* **53** (1996) 2752–2780, [arXiv:hep-ph/9509255](#).
 - [21] M. Malinsky, J. C. Romao, and J. W. F. Valle, “Novel supersymmetric SO(10) seesaw mechanism,” *Phys. Rev. Lett.* **95** (2005) 161801, [arXiv:hep-ph/0506296](#).
 - [22] A. Pilaftsis, “CP violation and baryogenesis due to heavy Majorana neutrinos,” *Phys. Rev. D* **56** (1997) 5431–5451, [arXiv:hep-ph/9707235](#).
 - [23] P.-H. Gu and U. Sarkar, “Leptogenesis with Linear, Inverse or Double Seesaw,” *Phys. Lett. B* **694** (2011) 226–232, [arXiv:1007.2323 \[hep-ph\]](#).
 - [24] M. J. Dolan, T. P. Dutka, and R. R. Volkas, “Dirac-Phase Thermal Leptogenesis in the extended Type-I Seesaw Model,” *JCAP* **06** (2018) 012, [arXiv:1802.08373 \[hep-ph\]](#).

- [25] C. Dib, S. Kovalenko, I. Schmidt, and A. Smetana, “Low-scale seesaw from neutrino condensation,” *Nucl. Phys. B* **952** (2020) 114910, [arXiv:1904.06280 \[hep-ph\]](#).
- [26] S. Blanchet, T. Hambye, and F.-X. Josse-Michaux, “Reconciling leptogenesis with observable $\mu \rightarrow e$ gamma rates,” *JHEP* **04** (2010) 023, [arXiv:0912.3153 \[hep-ph\]](#).
- [27] S. Blanchet, P. S. B. Dev, and R. N. Mohapatra, “Leptogenesis with TeV Scale Inverse Seesaw in SO(10),” *Phys. Rev. D* **82** (2010) 115025, [arXiv:1010.1471 \[hep-ph\]](#).
- [28] A. E. C. Hernández, D. T. Huong, and I. Schmidt, “Universal inverse seesaw mechanism as a source of the SM fermion mass hierarchy,” *Eur. Phys. J. C* **82** no. 1, (2022) 63, [arXiv:2109.12118 \[hep-ph\]](#).
- [29] A. E. C. Hernández, C. Espinoza, J. C. Gómez-Izquierdo, and M. Mondragón, “Fermion masses and mixings, dark matter, leptogenesis and $g - 2$ muon anomaly in an extended 2HDM with inverse seesaw,” *Eur. Phys. J. Plus* **137** no. 11, (2022) 1224, [arXiv:2104.02730 \[hep-ph\]](#).
- [30] A. E. C. Hernández and I. Schmidt, “A renormalizable left-right symmetric model with low scale seesaw mechanisms,” *Nucl. Phys. B* **976** (2022) 115696, [arXiv:2101.02718 \[hep-ph\]](#).
- [31] A. Abada, N. Bernal, A. E. Cárcamo Hernández, S. Kovalenko, and T. B. de Melo, “Three-Loop Inverse Scotogenic Seesaw Models,” [arXiv:2312.14105 \[hep-ph\]](#).
- [32] A. E. Cárcamo Hernández, R. Martínez, and F. Ochoa, “Fermion masses and mixings in the 3-3-1 model with right-handed neutrinos based on the S_3 flavor symmetry,” *Eur. Phys. J. C* **76** no. 11, (2016) 634, [arXiv:1309.6567 \[hep-ph\]](#).
- [33] A. E. Cárcamo Hernández, S. Kovalenko, H. N. Long, and I. Schmidt, “A variant of 3-3-1 model for the generation of the SM fermion mass and mixing pattern,” *JHEP* **07** (2018) 144, [arXiv:1705.09169 \[hep-ph\]](#).
- [34] A. E. Cárcamo Hernández, H. N. Long, and V. V. Vien, “The first $\Delta(27)$ flavor 3-3-1 model with low scale seesaw mechanism,” *Eur. Phys. J. C* **78** no. 10, (2018) 804, [arXiv:1803.01636 \[hep-ph\]](#).
- [35] A. E. Cárcamo Hernández, N. A. Pérez-Julve, and Y. Hidalgo Velásquez, “Fermion masses and mixings and some phenomenological aspects of a 3-3-1 model with linear seesaw mechanism,” *Phys. Rev. D* **100** no. 9, (2019) 095025, [arXiv:1907.13083 \[hep-ph\]](#).
- [36] A. E. Cárcamo Hernández, Y. Hidalgo Velásquez, and N. A. Pérez-Julve, “A 3-3-1 model with low scale seesaw mechanisms,” *Eur. Phys. J. C* **79** no. 10, (2019) 828, [arXiv:1905.02323 \[hep-ph\]](#).
- [37] A. E. Cárcamo Hernández, D. T. Huong, and H. N. Long, “Minimal model for the fermion flavor structure, mass hierarchy, dark matter, leptogenesis, and the electron and muon anomalous magnetic moments,” *Phys. Rev. D* **102** no. 5, (2020) 055002, [arXiv:1910.12877 \[hep-ph\]](#).
- [38] A. E. Cárcamo Hernández, J. W. F. Valle, and C. A. Vaquera-Araujo, “Simple theory for scotogenic dark matter with residual matter-parity,” *Phys. Lett. B* **809** (2020) 135757, [arXiv:2006.06009 \[hep-ph\]](#).
- [39] A. E. Cárcamo Hernández, S. Kovalenko, F. S. Queiroz, and Y. S. Villamizar, “An extended 3-3-1 model with radiative linear seesaw mechanism,” *Phys. Lett. B* **829** (2022) 137082, [arXiv:2105.01731 \[hep-ph\]](#).
- [40] A. E. C. Hernández, C. Hati, S. Kovalenko, J. W. F. Valle, and C. A. Vaquera-Araujo, “Scotogenic neutrino masses with gauged matter parity and gauge coupling unification,” *JHEP* **03** (2022) 034, [arXiv:2109.05029 \[hep-ph\]](#).
- [41] M. Malinsky, T. Ohlsson, Z.-z. Xing, and H. Zhang, “Non-unitary neutrino mixing and CP violation in the minimal inverse seesaw model,” *Phys. Lett. B* **679** (2009) 242–248, [arXiv:0905.2889 \[hep-ph\]](#).
- [42] A. Abada and M. Lucente, “Looking for the minimal inverse seesaw realisation,” *Nucl. Phys. B* **885** (2014) 651–678, [arXiv:1401.1507 \[hep-ph\]](#).
- [43] F. F. Deppisch, P. S. Bhupal Dev, and A. Pilaftsis, “Neutrinos and Collider Physics,” *New J. Phys.* **17** no. 7, (2015) 075019, [arXiv:1502.06541 \[hep-ph\]](#).
- [44] A. Abada, N. Bernal, A. E. C. Hernández, X. Marcano, and G. Piazza, “Gauged inverse seesaw from dark matter,” *Eur. Phys. J. C* **81** no. 8, (2021) 758, [arXiv:2107.02803 \[hep-ph\]](#).
- [45] C. Bonilla, A. E. Cárcamo Hernández, S. Kovalenko, H. Lee, R. Pasechnik, and I. Schmidt, “Fermion mass hierarchy in an extended left-right symmetric model,” *JHEP* **12** (2023) 075, [arXiv:2305.11967 \[hep-ph\]](#).
- [46] C. Bonilla, A. E. Cárcamo Hernández, B. Saez Diaz, S. Kovalenko, and J. Marchant Gonzalez, “Dark matter from a radiative inverse seesaw majoron model,” *Phys. Lett. B* **847** (2023) 138282, [arXiv:2306.08453 \[hep-ph\]](#).
- [47] D. Chang and H. N. Long, “Interesting radiative patterns of neutrino mass in an SU(3)(C) x SU(3)(L) x U(1)(X) model with right-handed neutrinos,” *Phys. Rev. D* **73** (2006) 053006, [arXiv:hep-ph/0603098](#).
- [48] J. Herrero-Garcia, M. Nebot, N. Rius, and A. Santamaria, “The Zee–Babu model revisited in the light of new data,” *Nucl. Phys. B* **885** (2014) 542–570, [arXiv:1402.4491 \[hep-ph\]](#).
- [49] K. L. McDonald and B. H. J. McKellar, “Evaluating the two loop diagram responsible for neutrino mass in Babu’s model,” [arXiv:hep-ph/0309270](#).
- [50] V. H. Binh, D. T. Binh, A. E. Cárcamo Hernández, D. T. Huong, D. V. Soa, and H. N. Long, “Higgs sector phenomenology in the 3-3-1 model with an axionlike particle,” *Phys. Rev. D* **107** no. 9, (2023) 095030, [arXiv:2007.05004 \[hep-ph\]](#).
- [51] **ATLAS, CMS Collaboration**, G. Aad *et al.*, “Measurements of the Higgs boson production and decay rates and constraints on its couplings from a combined ATLAS and CMS analysis of the LHC pp collision data at $\sqrt{s} = 7$ and 8 TeV,” *JHEP* **08** (2016) 045, [arXiv:1606.02266 \[hep-ex\]](#).
- [52] E. W. Kolb and M. S. Turner, *The Early Universe*, vol. 69. 1990.
- [53] M. Blennow, E. Fernández-Martínez, J. Hernández-García, J. López-Pavón, X. Marcano, and D. Naredo-Tuero, “Bounds on lepton non-unitarity and heavy neutrino mixing,” *JHEP* **08** (2023) 030, [arXiv:2306.01040 \[hep-ph\]](#).
- [54] R. A. Diaz, R. Martínez, and J. A. Rodríguez, “Phenomenology of lepton flavor violation in 2HDM(3) from $(g-2)(\mu)$

- and leptonic decays,” *Phys. Rev.* **D67** (2003) 075011, [arXiv:hep-ph/0208117 \[hep-ph\]](#).
- [55] F. Jegerlehner and A. Nyffeler, “The Muon $g-2$,” *Phys. Rept.* **477** (2009) 1–110, [arXiv:0902.3360 \[hep-ph\]](#).
 - [56] C. Kelso, H. N. Long, R. Martinez, and F. S. Queiroz, “Connection of $g - 2_\mu$, electroweak, dark matter, and collider constraints on 331 models,” *Phys. Rev.* **D90** no. 11, (2014) 113011, [arXiv:1408.6203 \[hep-ph\]](#).
 - [57] M. Lindner, M. Platscher, and F. S. Queiroz, “A Call for New Physics : The Muon Anomalous Magnetic Moment and Lepton Flavor Violation,” *Phys. Rept.* **731** (2018) 1–82, [arXiv:1610.06587 \[hep-ph\]](#).
 - [58] K. Kowalska and E. M. Sessolo, “Expectations for the muon $g-2$ in simplified models with dark matter,” *JHEP* **09** (2017) 112, [arXiv:1707.00753 \[hep-ph\]](#).
 - [59] **Muon $g-2$** Collaboration, D. P. Aguillard *et al.*, “Measurement of the Positive Muon Anomalous Magnetic Moment to 0.20 ppm,” *Phys. Rev. Lett.* **131** no. 16, (2023) 161802, [arXiv:2308.06230 \[hep-ex\]](#).
 - [60] L. Morel, Z. Yao, P. Cladé, and S. Guellati-Khélifa, “Determination of the fine-structure constant with an accuracy of 81 parts per trillion,” *Nature* **588** no. 7836, (2020) 61–65.